

1 **Storm-triggered landslides in the Peruvian Andes and implications for topography,**  
2 **carbon cycles, and biodiversity**

3 Kathryn E. Clark<sup>1\*</sup>, A. Joshua West<sup>2</sup>, Robert G. Hilton<sup>3</sup>, Gregory P. Asner<sup>4</sup>, Carlos A.  
4 Quesada<sup>5</sup>, Miles R. Silman<sup>6</sup>, Sassan S. Saatchi<sup>7</sup>, William Farfan-Rios<sup>6</sup>, Roberta E. Martin<sup>4</sup>,  
5 Aline B. Horwath<sup>8</sup>, Kate Halladay<sup>1</sup>, Mark New<sup>1,9</sup> and Yadvinder Malhi<sup>1</sup>

6 <sup>1</sup> Environmental Change Institute, School of Geography and the Environment, University of  
7 Oxford, Oxford, UK.

8 (\*correspondance: kathryn.clark23@gmail.com; Current address: Department of Earth and  
9 Environmental Science, University of Pennsylvania, Philadelphia, PA, USA)

10 <sup>2</sup> Department of Earth Sciences, University of Southern California, Los Angeles, CA, USA.

11 <sup>3</sup> Department of Geography, Durham University, Durham, UK.

12 <sup>4</sup> Department of Global Ecology, Carnegie Institution for Science, Stanford, CA, USA.

13 <sup>5</sup> Instituto Nacional de Pesquisas da Amazônia, Manaus, Brazil.

14 <sup>6</sup> Department of Biology and Center for Energy, Environment, and Sustainability, Wake  
15 Forest University, Winston-Salem, NC, USA.

16 <sup>7</sup> Jet Propulsion Laboratory, California Institute of Technology, Pasadena, CA, USA.

17 <sup>8</sup> Department of Plant Sciences, University of Cambridge, Cambridge, UK.

18 <sup>9</sup> African Climate and Development Initiative, University of Cape Town, Rondebosch, Cape  
19 Town, South Africa.

20 **Abstract**

21 In this study, we assess the geomorphic role of a rare, large-magnitude landslide-triggering event and  
22 consider its effect on mountain forest ecosystems and the erosion of organic carbon in an Andean  
23 river catchment. Proximal triggers such as large rain storms are known to cause large numbers of  
24 landslides, but the relative effects of such low-frequency, high-magnitude events are not well known  
25 in the context of more regular, smaller events. We develop a 25-year duration, annual-resolution  
26 landslide inventory by mapping landslide occurrence in the Kosñipata Valley, Peru, from 1988 to  
27 2012 using Landsat, Quickbird and Worldview satellite images. Catchment-wide landslide rates were  
28 high, at  $0.076\% \text{ yr}^{-1}$  by area. As a result, landslides on average completely turn over hillslopes every  
29  $\sim 1320$  years, although our data suggest that landslide occurrence varies spatially, such that turnover  
30 times are likely to be non-uniform. In total, landslides stripped  $26 \pm 4 \text{ tC km}^{-2} \text{ yr}^{-1}$  of organic carbon  
31 from soil (80%) and vegetation (20%) during the study period. A single rain storm in March 2010  
32 accounted for 27% of all landslide area observed during the 25-year study and accounted for 26% of  
33 the landslide-associated organic carbon flux. An approximately linear magnitude-frequency  
34 relationship for annual landslide areas suggests that large storms contribute an equivalent landslide  
35 failure area to the sum of smaller frequency landslides events occurring over the same period.  
36 However, the spatial distribution of landslides associated with the 2010 storm is distinct. On the basis  
37 of precipitation statistics and landscape morphology, we hypothesize that focusing of storm-triggered  
38 landslide erosion at lower elevations in the Kosñipata catchment may be characteristic of longer-term  
39 patterns. These patterns may have implications for the source and composition of sediments and  
40 organic material supplied to river systems of the Amazon basin, and, through focusing of regular  
41 ecological disturbance, for the species composition of forested ecosystems in the region.

## 42 **1. Introduction**

43 Landslides are major agents of topographic evolution (e.g., Li et al., 2014; Egholm et al., 2013;  
44 Ekström and Stark, 2013; Larsen and Montgomery, 2012; Roering et al., 2005; Hovius et al., 1997)  
45 and are increasingly recognized for their important biogeochemical and ecological role in  
46 mountainous environments because they drive erosion of carbon and nutrients (Pepin et al., 2013;  
47 Ramos Scharrón et al., 2012; Hilton et al., 2011; West et al., 2011; Stallard, 1985) and introduce  
48 regular cycles of disturbance to ecosystems (Restrepo et al., 2009; Bussmann et al., 2008). Landslides  
49 result when slope angles reach a failure threshold (Burbank et al., 1996; Schmidt and Montgomery,  
50 1995; Selby, 1993), which is thought to occur in mountains as rivers incise their channels, leaving  
51 steepened hillslopes (Montgomery, 2001; Gilbert, 1877). Landsliding acts to prevent progressive  
52 steepening beyond a critical failure angle for bedrock, even as rivers continue to cut downwards  
53 (Larsen and Montgomery, 2012; Montgomery and Brandon, 2002; Burbank et al., 1996). However,  
54 many slopes prone to landslide failure may remain stable until a proximal triggering event, such as a  
55 storm (Lin et al., 2008; Meunier et al., 2008; Restrepo et al., 2003; Densmore and Hovius, 2000) or a  
56 large earthquake (Li et al., 2014; Dadson et al., 2004; Keefer, 1994). Intense storms can increase pore  
57 pressure from heavy rainfall (Terzaghi, 1951), decreasing soil shear strength and resulting in slope  
58 failure (Wang and Sassa, 2003).

59 By clearing whole sections of forest and transporting materials downslope, landslides can drive fluxes  
60 of organic carbon from the biosphere (Hilton et al., 2011; West et al., 2011; Restrepo and Alvarez,  
61 2006), delivering the carbon either into sediments (where recently photosynthesized carbon can be  
62 locked away) or into the atmosphere, if ancient organic material in bedrock or soils is exposed and  
63 oxidized (Hilton et al., 2014). Links between storm frequency, landslide occurrence, and carbon  
64 fluxes could generate erosion-carbon cycle-climate feedbacks (West et al., 2011; Hilton et al., 2008a).  
65 Moreover, storm-triggered landslides may link climate to forest disturbance, with implications for  
66 ecosystem dynamics (Restrepo et al., 2009). However, for storm-triggered landslides to keep  
67 occurring over prolonged periods of time, hillslopes must remain sufficiently steep, which typically  
68 occurs in mountains via sustained river incision. Incision is also climatically regulated (Ferrier et al.,  
69 2013), providing a mechanism connecting storm activity, erosion, and topographic evolution (e.g.,  
70 Bilderback et al., 2015), and further linking to organic carbon removal from hillslopes and ecological  
71 processes across landscapes.

72 In this study, we mapped landslides in a mountainous catchment in the Andes of Peru over a 25-year  
73 period, including one year (2010) in which a large storm triggered a numerous landslides. We  
74 quantify landslide rates on an annual basis and use comprehensive datasets on soil and above- and  
75 below-ground biomass to determine the amount of organic carbon stripped from hillslopes. We assess  
76 the relative landslide ‘work,’ in terms of total landslide area, done in different years to explore the

77 roles of varying magnitudes and frequencies of triggering events, providing a longer-term context for  
78 understanding storm-triggered landslides that has not been available in much of the prior research on  
79 storm effects. We also evaluate the spatial distribution of landslides with respect to catchment  
80 topography and climatic factors that may act as potential longer-term forcing on the location of most  
81 active landslide erosion. Finally, we assess the potential role of these spatial patterns in shaping  
82 regional topography, determining the composition of sediment delivered to rivers, and influencing  
83 forest ecosystems that are repeatedly disturbed by landslide occurrence.

84

## 85 **2. Study area**

86 The Kosñipata River (Fig. 1) is situated in the Eastern Andes of Peru. We focus on the catchment area  
87 upstream of a point (13°3'27"S 71°32'40"W) just downriver of San Pedro. Elevation in the catchment  
88 ranges from 1200 metres above sea level (m) to 4000 m, with a mean elevation ( $\pm 1$  standard  
89 deviation) of  $2700 \pm 600$  m and a catchment area of 185 km<sup>2</sup>. The forested area covers 150 km<sup>2</sup> and  
90 consists of tropical montane cloud forest at high elevations and sub-montane tropical rainforest at  
91 lower elevations (Fig. 1a) (Horwath, 2011). The area of puna grasslands covers 35 km<sup>2</sup> above the  
92 timberline at 3300 $\pm$ 250 m range. The valley is partially contained in Manu National Park, where  
93 logging is prohibited. A single unpaved road is located in the valley stretching from high to low  
94 elevations. The Kosñipata River flows through the study area and into the Alto Madre de Dios River,  
95 which feeds the Madre de Dios River, a tributary of the Amazon River. There are extensive datasets  
96 on plants, soil, ecosystem productivity, carbon and nutrient cycling and climate within the catchment  
97 (Malhi et al., 2010). Tree species richness ranges from 40 to 180 species ha<sup>-1</sup> for trees  $\geq 10$ cm diameter  
98 at breast height (dbh), and total forest C-stocks (Gurdak et al., 2014; Girardin et al., 2013; Horwath,  
99 2011; Gibbon et al., 2010) are representative of the wider Andean region (Saatchi et al., 2011).

100 The South American Low Level Jet carries humid winds westward over the Amazon Basin and then  
101 south along the flank of the Andes, driving orographic rainfall in the Eastern Cordillera of the Central  
102 Andes (Espinoza et al., 2015; Lowman and Barros, 2014; Marengo et al., 2004). In the study area,  
103 precipitation ranges from 2000 to 5000 mm yr<sup>-1</sup> and is highest at the lowest elevations, decreasing  
104 approximately linearly with the increase in elevation (Clark et al., 2014; Girardin et al., 2014b;  
105 Huaraca Huasco et al., 2014). Much of the valley has >75% cloud cover throughout the year in a band  
106 of persistent cloud that spans much of the Eastern Andes, although cloud immersion is restricted to  
107 elevations  $> \sim 1600$  m (Halladay et al., 2012) (Fig. 1a).

108 The Kosñipata Valley is in the tectonically active setting of the uplifting Eastern Cordillera of the  
109 Central Andes, associated with subduction of the Nazca Plate under the South American Plate  
110 (Gregory-Wodzicki, 2000). Since 1978, there have been  $\sim 4$  registered earthquakes larger than

111 magnitude  $M=5$  within a distance of 65 km from the Kosñipata Valley (Fig. 1b; USGS, 2013a;  
112 Gregory-Wodzicki, 2000), though significant ground shaking within the Kosñipata Valley has not  
113 been reported during the study interval. The Cusco fault zone is the nearest seismically active region,  
114 ~50 km southwest of the study site, consisting of normal faults stretching 200 km long and 15 km  
115 wide parallel to the Andean plateau (Cabrera et al., 1991) and where deep earthquakes are common  
116 (USGS, 2013a; Tavera and Buforn, 2001). In the Andean foothills, ~20 km northeast of the study site,  
117 there is an active fold and thrust belt (Vargas Vilchez and Hipolito Romero, 1998; Sébrier et al.,  
118 1985). The bedrock geology in the Kosñipata Valley is representative of the wider Eastern Andes  
119 (Clark et al., 2013). The catchment is dominated by metamorphosed sedimentary rocks in the high  
120 elevations (mostly mudstone protoliths of ~450 Ma) and a plutonic region in the lower elevations  
121 (Carlotto Caillaux et al., 1996; Fig. 1b).

122 Landslides are a pervasive feature of the landscape in the Kosñipata Valley. In general in the Andes,  
123 landslides are a common geomorphic process, with landslide area covering 1-6% of mountain  
124 catchments in parts of Ecuador and Bolivia (Blodgett and Isacks, 2007; Stoyan, 2000), and landslide-  
125 associated denudation rates have been estimated in the range of  $9\pm 5$  mm yr<sup>-1</sup> (Blodgett and Isacks,  
126 2007). Downstream of the Kosñipata River, detrital cosmogenic nuclide concentrations in river  
127 sediments in the Madre de Dios River suggest a denudation rate of ~0.3 mm yr<sup>-1</sup> (Wittmann et al.,  
128 2009), although this catchment includes a large lowland floodplain area. Cosmogenic-derived total  
129 denudation rates in the high Bolivian Andes range up to ~1.3 mm yr<sup>-1</sup> (Safran et al., 2005) and  
130 suspended sediment derived erosion rates up to 1.2 mm yr<sup>-1</sup> (Pepin et al., 2013). The difference  
131 between the landslide-associated erosion rates measured in Bolivia (Blodgett and Isacks, 2007) and  
132 the catchment-averaged denudation rates typical of this region has not been widely considered, and a  
133 more systematic comparison including data paired from identical catchments could offer fruitful  
134 avenues for further investigation. For purposes of this study, the observation of relatively high  
135 landslide rates suggests at the least that landslides are the primary mechanism of hillslope mass  
136 removal, as they are in other active mountain belts (Hovius et al., 2000; Hovius et al., 1997).

137

### 138 **3. Materials and methods**

#### 139 **3.1. Landslide mapping**

140 Landslides within the Kosñipata Valley were manually mapped over a 25-year period from 1988 to  
141 2012 using Landsat 5 (Landsat Thematic Mapper) and Landsat 7 (Landsat Enhanced Thematic  
142 Mapper Plus) satellite images (Fig. 2a) (USGS, 2013b). There were 38 usable Landsat images for the  
143 region over the 25-year period, with 1-3 available for each year (see Supplement Table S1). All  
144 images were acquired in the dry season (May-October). Landsat images were processed with a  
145 Standard Terrain Correction (Level 1T) which consists of systematic radiometric and geometric

146 processing using ground control points and a digital elevation model (DEM) for ortho-georectification  
147 (USGS, 2013b). The high frequency of the Landsat images made it possible to develop a time series  
148 of individual landslides over the entire 25-year duration which has not typically been achieved before  
149 in studies at the catchment-scale (Hilton et al., 2011; Hovius et al., 1997).

150 The landslide inventory was produced by manually mapping landslide scars and their deposits in  
151 ArcGIS and by verifying via ground-truthing of scars in the field. Mapping involved visually  
152 comparing images from one year to the next evaluating contrasting colour changes suggesting a  
153 landslide had occurred. A composite image of Landsat bands 5 (near-infrared, 1.55-1.75  $\mu\text{m}$ ), 3  
154 (visible red, 0.63-0.69  $\mu\text{m}$ ) and 7 (mid-infrared, 2.08-2.35  $\mu\text{m}$ ) was used in order to identify landslide  
155 scars with the greatest spectral difference to forest. Bedrock outcrops are minimal in the valley and  
156 thus not subject to mislabelling as landslides. Several aerial photographs (from 1963 and 1985) were  
157 used to identify and remove pre-1988 landslides from this study.

158 The landslide areas visible via spectral contrast in the Landsat images include regions of failure, run-  
159 out areas, and deposits. In some of the high-resolution imagery, we were able to distinguish scars  
160 from deposits, but not systematically enough to separately categorize these for the full landslide  
161 catalogue in this study. One 2007 landslide was coupled to a particularly large debris flow and stood  
162 out within our inventory, with the 1.7 km long debris flow comprising ~5% of the total landslide area  
163 for the total inventory from 1988 to 2012. With this one exception, we consider all areas with visible  
164 contrast outside of river channels as being “landslide” area (e.g., see Fig. 2a and inset photo). For the  
165 purposes of quantifying biomass disturbance and organic carbon fluxes associated with landslide  
166 activity, the convolution of scars and deposits is justified on the basis that all of these areas were  
167 covered in forest prior to landslide occurrence. However, the fate of carbon from scars vs. deposits  
168 may differ, as discussed below, and when considering the slope distribution of landslide areas, the  
169 deposit areas introduce some bias (see further discussion in Section 4.2, below). Future landslide  
170 mapping work, taking advantage of even higher resolution imagery than available in this study, would  
171 benefit from the effort to explicitly distinguish scars and deposits for full inventories.

172 The Landsat images had a mean visibility of 67% that varied year-to-year (Table S2; Fig. 3a). Non-  
173 visible portions were due to topographic shadow, cloud shadow, and no-data strips on Landsat 7  
174 images post-2002 (following failure of the satellite’s scan line corrector). Duplicate or triplicate  
175 images were used in most years, and so landslides obscured by cloud shadow or no-data were likely to  
176 be spotted within a year of their occurrence. Topographic shadow produced by hillslopes covered a  
177 minimum of 21% of the study area (35 km<sup>2</sup> out of 185 km<sup>2</sup>), predominantly on southwest facing  
178 slopes (223±52° azimuth), and was consistently present between images. Landslides that fell within  
179 these shadow areas were not visible. Using Quickbird imagery from 2005 (which covers 54% of the  
180 study area) we found that the Landsat topographic shadow areas have a similar area covered by

181 landslides as the visible areas; 26% of the Quickbird-mapped landslide area fell within Landsat  
182 topographic shadow areas, and these areas encompass a similar 22% of the total image area. We thus  
183 infer that landslide occurrence under Landsat topographic shadow is approximately equivalent to that  
184 in the visible portion of the Landsat images. On this basis, we estimate an error of  $< \sim 20\%$  in our  
185 landslide inventory due to missed landslides under topographic shadow.

186 Small-area landslides are not fully accounted for by our mapping approach due to the Landsat grid-  
187 resolution of 30 m x 30 m (Stark and Hovius, 2001). In addition, Landsat images may not allow  
188 distinguishing of clumped landslides (cf. Marc and Hovius, 2015; Li et al., 2014). We assessed the  
189 potential bias by comparing the Landsat imagery with Quickbird imagery from 2005 (at 2.4 m x 2.4 m  
190 resolution). Specifically, we compared landslides mapped from portions of 2005 Quickbird image that  
191 are visible in the Landsat imagery (i.e., not in topographic shadow, discussed above) with the  
192 Landsat-derived landslides mapped from 1988 to 2005 that had not recovered by 2005. The difference  
193 in landslide area is 181,760 m<sup>2</sup>, equivalent to  $\sim 25\%$  of the total landslide area. The area-frequency  
194 relationships (cf. Malamud et al., 2004 and references therein) for the two datasets show similar  
195 power law relationships for large landslides (Fig. 4) and illustrate that the different total landslide  
196 areas can be attributed mainly to missing small landslides ( $< 4,000$  m<sup>2</sup>) in the Landsat-derived maps.  
197 These small landslides contribute  $\sim 80\%$  of the observed difference, with the remaining difference  
198 attributable to 3 larger landslides (total area 30,500 m<sup>2</sup>) missed due to other reasons such as image  
199 quality. Based on the difference between total landslide area mapped via Quickbird vs. Landsat  
200 imagery, we estimate an error of  $\sim 20\%$  in our landslide inventory from missing small landslides and  
201  $< 5\%$  error from missing larger landslides.

### 202 **3.2 Landslide rates, turnover times, and landslide susceptibility**

203 We calculated landslide rate ( $R_{ls}$ , % yr<sup>-1</sup>) as the percentage of landslide area ( $A_{ls}$ ) per unit catchment  
204 area ( $A_{catchment}$ ), i.e.,  $R_{ls} = 100 \times A_{ls}/A_{catchment} \times 1/25$  yr for all landslide area observed during the 25-  
205 year study period. To assess the spatial distribution of landslides throughout the study area, we  
206 determined rates by 1 km<sup>2</sup> grid cells (Fig. 2b).

207 The average rate of slope turnover due to landslides ( $t_{ls}$ ) is the inverse of landslide rate. This metric  
208 reflects the time required for landslides to impact all of the landscape, solely based on their rate of  
209 occurrence (Hilton et al., 2011; Restrepo et al., 2009).  $t_{ls}$  was quantified over the visible portion of the  
210 study area in 1 km<sup>2</sup> cells (Fig. 2c).

211 To assess how landslide rate varies with elevation and hillslope angle, we divided each landslide  
212 polygon into 3 m x 3 m cells consistent with the Carnegie Airborne Observatory (CAO) digital  
213 elevation model (DEM) (Asner et al., 2012; see Appendix A). We used the resulting 3 m grid to  
214 calculate histograms of landslide areas and total catchment area as a function elevation and slope  
215 using 300 m and 1° intervals, respectively (Figs. 5, 6). We also defined landslide susceptibility ( $S_{ls}$ )

216 for a given range of elevation or slope angle values, as the ratio of the number of landslide cells in  
217 each elevation (or slope) range, divided by the total number of catchment cells in the equivalent  
218 range. Consistent with the landslide rate analysis, we only used catchment cells in the portion of the  
219 study area visible in the Landsat images.

### 220 **3.3. Calculation of carbon stripped from hillslopes by landslides**

#### 221 **3.3.1. General approach to calculating landslide-associated carbon fluxes**

222 We seek to quantify the amount of organic carbon mobilised by landslides at the catchment scale.  
223 This requires knowledge of the spatial distribution of carbon stocks on forested hillslopes at this scale.  
224 One approach is to use forest inventory maps derived from field surveys, aerial imagery, or other  
225 remote sensing observations (Asner et al., 2010; Saatchi et al., 2007) along with mapped landslides  
226 (e.g., Ramos Scharrón et al., 2012; West et al., 2011). However, such forest inventories do not  
227 typically capture below-ground or soil carbon stocks, the latter of which can make up the majority of  
228 total organic carbon in the landscape (Eswaran et al., 1993). Maps of soil C can be estimated from soil  
229 surveys together with knowledge of the C content in each soil type (Ramos Scharrón et al., 2012), but  
230 sufficiently detailed soil surveys are often unavailable and it is also difficult to test the key assumption  
231 that C content is constant for a given soil type.

232 An alternative approach, which we adopt in this study, is to use empirical trends in C stocks as a  
233 function of elevation, and to assign landslide area at a given elevation with a C stock value  
234 representative of that elevation (Hilton et al., 2011). Scatter in the relationship between elevation and  
235 C stocks (cf. Fig. 7, Table 1) means these trends do not provide the basis for a robust map of C stocks,  
236 nor a precise value for any single individual landslide. However, landslides in a setting like the  
237 Kosñipata Valley occur distributed across the catchment area at a given elevation, and the large  
238 number of landslides effectively samples from the observed scatter in C stocks. This averaging means  
239 that, when we sum together estimates of C stock stripped by all landslides across the catchment, we  
240 can estimate a representative mean value for the total flux of landslide-associated carbon. An implicit  
241 assumption is that there is not a systematic, coincident spatial bias in both landslide location and C  
242 stock at a given elevation (e.g., see discussion of potential slope biases on C stock estimates, below).

#### 243 **3.3.2. Carbon stocks as a function of elevation**

244 To constrain trends in C stocks with elevation in the Kosñipata catchment, we collated soil and  
245 vegetation datasets, taking advantage of the numerous plot studies. The datasets consist of soil carbon  
246 stocks, above ground living biomass (trees), and root carbon stocks (Girardin et al., 2010). Each  
247 dataset consisted of data from 6 to 13 plots along the altitudinal gradient (Fig. 7). Linear regressions  
248 of C stock ( $\text{tC km}^{-2}$ ) versus elevation (m) were determined for the soil, above ground living biomass,  
249 and roots separately (Hilton et al., 2011) and are reported in Table 1. For above ground living



250 biomass, we assumed a wood carbon concentration of 46% measured in stems and leaves ( $n = 130$ )  
251 throughout the Kosñipata Valley (Rao, 2011). The trend in above ground biomass versus elevation  
252 from this dataset fits within the range reported by Asner et al. (2014). Additionally, data on wood  
253 debris carbon stocks (Gurdak et al., 2014), and epiphyte carbon stocks (Horwath, 2011) are available  
254 but were not used in the carbon stock analysis because: (i) these comprise a small proportion of the  
255 total biomass (see below), and (ii) do not show systematic change with elevation, precluding the use  
256 of our elevation-based approach for these biomass components.

257 For soil organic carbon (SOC) stocks, we used data from soil pits along the altitudinal gradient. Pits  
258 were dug at 11 forest plots, each with 6 to 51 individual soil pits per plot. Soil pits were dug from the  
259 surface at 0.05 to 0.5 m depth intervals until reaching bedrock, which was typically found at  $\sim 1$  m  
260 depth (see Supplement Table S3). Carbon stocks were determined by multiplying interval depth (m)  
261 and measured soil organic carbon content (%OC) by bulk density ( $\text{g cm}^{-3}$ ) for each soil layer. %OC  
262 was measured at each layer for every pit. For each plot one pit was measured for bulk density at the  
263 following intervals: 0-5, 5-10, 10-20, 20-30, 30-50, 50-100, 100-150 cm, and the depth-density trend  
264 from this pit was applied to other pits from the same plot. Soils were collected and processed  
265 following the methods Quesada et al. (2010). An average SOC stock (in  $\text{tC km}^{-2}$ ) for each plot was  
266 determined from the mean of individual pit SOC stocks (Fig. 7a; Table S3).

267 Compared to previously published SOC data for this region, this dataset is the most complete,  
268 encompassing more pits per plot and considering the full soil depth. Prior studies have considered the  
269 SOC stock over a uniform 0-30 cm depth (e.g., Girardin et al., 2014a) or considering separate  
270 horizons to a depth of 50 cm (Zimmermann et al., 2009). Our soil C stock values are a factor of 1.2 to  
271 1.7 higher than values reported in these previous studies (Girardin et al., 2014a; Zimmermann et al.,  
272 2009). For the same soil pit data (i.e., density and %C) used in this study, calculation of soil C stocks  
273 over depths equivalent to those used in the prior studies (i.e., over the top 0-30 cm and 0-50 cm)  
274 yields values in close agreement with those previously reported (see Supplement Fig. S1). This  
275 consistency indicates that the differences between the full-depth values used here, versus the partial  
276 depth values reported previously, are attributable predominantly to the integration depth used.

277 We use the SOC stock data to estimate the amount of soil carbon removed by landslides. These data  
278 may provide an upper estimate on the total amount of organic carbon derived from recently  
279 photosynthesized biomass (i.e., “biospheric organic carbon”), partly because of the presence of  
280 carbonate C and rock-derived organic carbon which is present in the catchment (Clark et al., 2013).  
281 However, the contribution from these non-biospheric components is expected to be small given the  
282 relatively low content of each compared to biospheric %OC, typically at concentrations of many  
283 percent. Additional bias may arise from the location of plots within the catchment, specifically with  
284 respect to topographic position (Marvin et al., 2014). The mean plot slopes range from  $20^\circ$  to  $38^\circ$ , as

285 measured from the 3 m x 3 m CAO DEM, so these sites capture a large slope range but are at the  
286 lower slope end of the slopes found throughout the Kosñipata catchment (mean catchment slope of  
287 38°). Data on soil OC stocks collected from a wide range in slopes at high elevations (near the tree  
288 line) in the region of the Kosñipata Valley suggest there is not an evident slope-dependence that  
289 would be likely to strongly bias our results (see Supplement Fig. S2; Gibbon et al., 2010).

290

### 291 **3.3.3. Calculating fluxes of carbon stripped from hillslopes by landslides**

292 Carbon stocks for soil, above ground living biomass, and roots were calculated for elevation bands of  
293 300 m, based on the relationships in Table 1. Landslide carbon flux ( $\text{tC yr}^{-1}$ ) was determined by  
294 multiplying the landslide rate in each elevation band ( $\% \text{ yr}^{-1}$ ) by soil, AGLB, and root carbon stocks  
295 ( $\text{tC km}^{-2}$ ) in the respective elevation band. We propagated the error on the elevation trends (from Fig.  
296 7 and Table 1) to estimate uncertainty on the landslide-associated carbon flux by Gaussian error  
297 propagation. The landslide C yield ( $\text{tC km}^{-2} \text{ yr}^{-1}$ ) was calculated by summing all 300 m elevation  
298 bands and normalising by the non-shadow catchment area ( $143 \text{ km}^2$ ).

299 The calculations assume that landslides strip all above ground, root biomass and soil material from  
300 hillslopes. This assumption is supported by field observations from the Kosñipata Valley that  
301 landslides are cleared of visible vegetation and roots and are typically bedrock failures that remove  
302 the entire mobile soil layer. To test this latter assumption, we used geometric scaling relationships for  
303 landslides in mountainous terrain (Larsen et al., 2010) to estimate landslide depths. We calculated  
304 landslide volume from the area (A)-volume (V) relationship,  $V = \alpha A^\gamma$ , where  $\alpha$  and  $\gamma$  are scaling  
305 parameters (we used  $\alpha = 0.146$  and  $\gamma = 1.332$ , from the compilation of global landslides in Larsen et  
306 al., 2010, but also tested other literature values). We estimated average depth by dividing volume for  
307 each landslide by the respective landslide area.

### 308 **3.4. Landslide revegetation**

309 We classified landslides as being “revegetated” when they were dominated by a closed forest canopy  
310 to an extent that we could no longer visually distinguish the landslide scar or bare ground in the 2 m  
311 resolution WorldView-2 imagery (Blodgett and Isacks, 2007). We determined the fraction of area of  
312 the landslides occurring in each year (beginning in 1988) that was no longer visible as of 2011, the  
313 year with the latest high-resolution image (Fig. 8). Some landslides were revegetated as soon as four  
314 years after occurrence. For landslide years prior to 2008, i.e. all landslide years with some observable  
315 recovery, we ran a linear regression between landslide area revegetated (specifically, area of fully  
316 revegetated landslides from a given year as a % of total landslide area from that year) and the number  
317 of years that had passed since landslide occurrence (the difference between the given year and 2011).

318 This analysis used a total of 18 data points, one for each year between 1988 and 2007 except for 2  
319 years that had no measured landslides (Fig. 8; Table S2).

320 The metric of visible revegetation that we use in this study provides a measurable index for assessing  
321 ecosystem recovery from remote imagery. However, it does not necessarily mean complete  
322 replenishment of above ground carbon stocks or regrowth of all vegetation to the extent present prior  
323 to landslide removal. It is also likely to take longer than this time for replenishment of soil carbon  
324 stocks to pre-landslide values (Restrepo et al., 2009).

### 325 **3.5. Topographic analysis**

326 We used two DEMs for topographic analysis. Slope angles and elevation statistics within the  
327 Kosñipata catchment study area were calculated from the 3m x 3m CAO LiDAR-based DEM (see  
328 Appendix A). For river channel analysis within the Kosñipata Valley and for all topographic analyses  
329 in the wider Madre de Dios region, we used a 30 m resolution SRTM-derived DEM (Farr et al., 2007)  
330 with holes patched using the ASTER GDEM (METI/NASA, 2009). We were not able to use the  
331 higher-resolution CAO DEM for these calculations because it did not extend beyond the Kosñipata  
332 catchment study area and contained gaps that made complete flow routing calculations problematic.

333 The dependence of calculated slope on grid resolution (Lin et al., 2008; Blodgett and Isacks, 2007;  
334 Zhang and Montgomery, 1994) means that reported slope values inherently differ between the DEMs  
335 used in this study, and when compared to values from the 90 m x 90 m SRTM-derived DEM (cf.  
336 Clark et al., 2013). In this study, we only compare results internally between values calculated from  
337 the same DEM.

338

## 339 **4. Results**

### 340 **4.1. Landslide rates and role of a large rain storm in 2010**

341 Approximately 2% (2.8 km<sup>2</sup>) of the visible Kosñipata Valley study area experienced landslides over  
342 the 25-year study period. This percentage of landslide area is similar to landslide coverage in the  
343 Ecuadorian and Bolivian Andes (Blodgett and Isacks, 2007; Stoyan, 2000). Of the total landslide area  
344 in the catchment, 97.1% was in the forested portion and the remaining 2.9% in the puna.

345 The mean valley-wide landslide rates were 0.076% yr<sup>-1</sup>, when averaged across 1 x 1 km grid cells.  
346 Rates ranged from no landslides detected to 0.85% yr<sup>-1</sup> for individual grid cells (Fig. 2b). The average  
347 landslide rate corresponds to average hillslope turnover time of ~1320 yrs for the valley (Fig. 2c).  
348 Values reported provide a minimum constraint on landslide rate and a maximum constraint on  
349 turnover time, since small landslides and landslides under topographic shadow were excluded (see  
350 Section 3.1). The landslide hillslope turnover time in the Kosñipata Valley is similar to the landslide

351 hillslope turnover time observed in the Waitangitona Basin of New Zealand, but is 2.3 times faster  
352 than the mean landscape-scale landslide hillslope turnover in the western Southern Alps of New  
353 Zealand (Hilton et al., 2011) and in Guatemala (Restrepo and Alvarez, 2006) and 24 times faster than  
354 in Mexico and in Central America (Restrepo and Alvarez, 2006).

355 A single large-magnitude rainfall event on March 4<sup>th</sup> 2010 triggered 27% of all of the landslide area  
356 observed during the 25-year study period in the Kosñipata study catchment. Rainfall during this storm  
357 peaked at 94 mm hr<sup>-1</sup>, with ~200 mm falling in 4 hr, recorded by a meteorology station at 1350 m  
358 within the catchment (Fig. 9). The storm accounted for ~185 landslides with 0.75 km<sup>2</sup> cumulative  
359 area. The annual total landslide area for 2010 was consequently much higher than for any other year  
360 in the dataset (Fig. 3).

#### 361 **4.2. Spatial patterns of landslides**

362 The histogram of catchment area in the Kosñipata catchment shows a skewed distribution with respect  
363 to elevation, with greater area at lower elevations (Fig. 5a). The histogram of landslide area is shifted  
364 to lower elevations compared to the catchment and shows a bi-modality. The 2010 landslides focused  
365 almost exclusively at low elevations, below ~2600 m (Fig. 5c). Although the remaining landslides  
366 over the 25-year study period located at low elevations relative to the catchment, they were at higher  
367 elevations than the 2010 landslides. The bi-modality of the overall landslide distribution emerges  
368 from the addition of the two nearly distinct distributions (Fig. 5c). Because of the small catchment  
369 area at low elevations, overall landslide susceptibility is highest at the low elevations (particularly  
370 <~1800 m) (Fig. 5b). When excluding the 2010 landslides, the high susceptibility at low elevations is  
371 not evident, and the only clear trend is the very low landslide susceptibility at the highest elevations  
372 (> 3500 m) (Fig. 5d). Since our mapping did not distinguish landslide scars from deposits (see  
373 Section 3.1), systematic changes in the ratio of scar to deposit area with elevation could influence  
374 apparent patterns of landslide occurrence. For example, larger deposit areas at low elevation would  
375 increase calculated susceptibility even if the total landslide scar area were not larger. However, our  
376 anecdotal field observations do not suggest that landslides at lower elevations have consistently longer  
377 run-out or larger deposit areas, so it is unlikely that such bias explains the observed relations between  
378 landslide occurrence and topography within our inventory.

379 The catchment area has a mean slope of 38° (calculated from the CAO DEM) and is skewed to lower  
380 slopes (Figs. 2d, 6a). The distribution of landslide areas is shifted to slightly higher slopes compared  
381 to catchment area and lacks the broad abundance at slopes <30°. The 2010 landslides show a similar  
382 distribution with respect to slope as the landslides from all other years (Fig. 6c). In all cases, landslide  
383 susceptibility increases sharply for slopes >30-40° (Fig. 6d). All of the landslide data include areas at  
384 low slopes, which we interpret as artefacts related to landslide deposits residing in valley bottoms,  
385 since our mapping routines did not distinguish scars from deposits.

### 386 **4.3. Catchment topographic characteristics**

387 The Kosñipata catchment is characterized by a prominent vertical step knickpoint between  
388 approximately 1600 and 1400 m elevation (Fig. 10a). This knickpoint marks an inflection in the  
389 relationship between upstream drainage area and the slope of the river channel, characteristic of the  
390 transition from colluvial to bedrock or alluvial channels in mountainous settings (Whipple, 2004;  
391 Montgomery and Buffington, 1997) although we recognize that processes such as debris-flow incision  
392 may also influence the form of these relations (Stock and Dietrich, 2003). We used flow routing to  
393 separate the catchment into those slopes that drain into the river system upstream of this transition  
394 zone (as defined by the elevation at the top of the vertical step knickpoint) and those slopes that drain  
395 into the river system downstream of the transition (Fig. 10b). Hillslope angles are, on average, steeper  
396 downstream of the transition than upstream, and the distribution of slope angles downstream lacks the  
397 prominent bulge at relatively low slopes that is observed upstream of the transition. The general  
398 features observed in the Kosñipata study catchment, specifically the transition in the slope-area curves  
399 and the related shift in hillslope angles, also generally characterize the other major rivers draining  
400 from the eastern flank of the Andes in the Alto Madre de Dios (Fig. 11).

### 401 **4.4. Catchment-scale carbon stocks and stripping of carbon by landslides**

402 The estimated catchment-scale carbon stock for the Kosñipata Valley is  $\sim 34\,670 \pm 4545$  tC km<sup>-2</sup>, with  
403  $\sim 27\,680 \pm 4420$  tC km<sup>-2</sup> in soil and  $\sim 5370 \pm 840$  tC km<sup>-2</sup> in vegetation (Fig. 7). We estimate that  
404 epiphyte (Horwath, 2011) and woody debris (Gurdak et al., 2014) biomass adds an additional  $\sim 7\%$  of  
405 carbon ( $<5\%$  from epiphytes and  $<3\%$  from woody debris; Fig. 7c). Overall, the vegetation carbon  
406 stock values from the Kosñipata Valley are slightly lower than lowland tropical forests, and the soil  
407 values higher (Dixon et al., 1994), which is consistent with broad trends in the tropics in which soil  
408 carbon stocks increase with elevation and are frequently greater than vegetation carbon stocks  
409 (Gibbon et al., 2010; Raich et al., 2006).

410 Averaged over the 25-year duration across the 143 km<sup>2</sup> non-shadowed catchment area, the estimated  
411 total flux of carbon stripped from hillslopes by landslides was  $3700 \pm 510$  tC yr<sup>-1</sup>, with  $2880 \pm 500$  tC yr<sup>-1</sup>  
412 <sup>1</sup> derived from soil and  $820 \pm 110$  tC yr<sup>-1</sup> from vegetation (Fig. 12a). In terms of area-normalized yield  
413 of carbon, landslides stripped  $26 \pm 4$  tC km<sup>-2</sup> yr<sup>-1</sup> from hillslopes, with  $20 \pm 3$  tC km<sup>-2</sup> yr<sup>-1</sup> derived from  
414 soil and  $5.7 \pm 0.8$  tC km<sup>-2</sup> yr<sup>-1</sup> from vegetation (Table 2; Fig. 12b). These values may underestimate  
415 total catchment-wide fluxes because our landslide mapping process missed a proportion of small,  
416 numerous landslides (see Fig. 4, Section 3.1).

417 On the other hand, our values may overestimate fluxes from soil OC if landslides are shallower than  
418 soil depths, since we have assumed complete stripping of soil material to full soil depth and since soil  
419 OC stocks depend on depth of integration (see Section 3.3, above). The deepest average soil depths  
420 observed in the plots used in this study were 1.58 m (Table S3). Using average scaling parameters for

421 global landslides (Larsen et al., 2010), only 99 landslides in our inventory, equating to 0.06 km<sup>2</sup> total  
422 landslide area (or ~2% of total landslide area), would be shallower than these deepest soils at 1.58 m.  
423 Using scaling parameters for bedrock landslides only ( $\alpha = 0.146$  and  $\gamma = 1.332$ ; Larsen et al. 2010,  
424 results in only one landslide shallower than 1.58 m. This analysis corroborates our field observations  
425 that most landslides in the Kosñipata Valley clear soil from hillslopes and expose bedrock. We thus  
426 view our calculation of fluxes on the basis of complete stripping of soil as providing a reasonable  
427 estimate.

428 Our calculation of landslide-associated carbon fluxes includes carbon that was previously residing  
429 both on landslide scars and in areas of landslide deposits. The fate of carbon from each of these areas  
430 may differ, but such differences are not well known and we consider all to contribute to the loss of  
431 previously living biomass as a result of landslide occurrence. When considering carbon budgets at the  
432 landscape-scale, the landslide-associated carbon fluxes we report here should also be viewed in the  
433 context that other processes such as soil creep may additionally contribute to the transfer of carbon  
434 from hillslopes to rivers (e.g., Yoo et al., 2005).

435

## 436 **5. Discussion**

### 437 **5.1. The geomorphic ‘work’ of storm-triggered landslides in the Kosñipata Valley**

438 The March 2010 storm clearly stands out as the most significant landslide event that occurred during  
439 the duration of this study. We lack a precipitation record for the full 25-year study period, but it is  
440 probable that this storm was the largest single precipitation event during that time. Landslides  
441 triggered in 2010 account for 0.75 km<sup>2</sup>, or 27% of the total landslide area during the 25-year study  
442 period, and these landslides stripped 25,500 tC from hillslopes, equivalent to 26% of the total. The  
443 quantitative importance of this individual storm in our dataset is consistent with observations of  
444 storm-triggering of intense landslides elsewhere (Wohl and Ogden, 2013; Ramos Scharrón et al.,  
445 2012; West et al., 2011; Casagli et al., 2006).

446 The annual resolution of our observations of landslide rates in the Kosñipata Valley makes it possible  
447 to consider how the geomorphic work done in this relatively infrequent but high magnitude event  
448 compares to the work done in smaller but more frequent events. Here we define geomorphic work,  
449 *sensu* Wolman and Miller (1960), as total landslide area, reflecting the removal of material from  
450 hillslopes (rather than, for example, the work done by landslides to modify slope angles). Across the  
451 25-year dataset, we estimate the return time or recurrence interval RI (i.e., how frequently a year of  
452 given total landslide magnitude would be expected to occur), as  $RI_i = (n+1)/m_i$ , where  $RI_i$  is the return  
453 interval for the year with the  $i^{\text{th}}$  largest total annual landslide area,  $n$  is the total length of the record  
454 (25 years in this study) and  $m_i$  is the rank order of year  $i$  within the dataset in terms of total landslide

455 area. Thus 2010, the year with most landslide area, has  $RI = 26$  years, while years characterized by  
456 lower landslide area have more frequent inferred recurrence intervals. When the annual data for  
457 landslide area are plotted as a function of  $RI$  (Fig. 3b), 2010 is clearly at the highest magnitude, as a  
458 result of the March 2010 storm. Even so, the landslide area from 2010 still falls on an approximately  
459 linear (power law exponent  $\sim 1$ ) trend coherent with the rest of the dataset. We do not have high  
460 enough temporal resolution to analyse the effects of individual storms in detail, as would be preferred  
461 for a robust recurrence interval analysis. Nonetheless, the linearity of the relationship for annual  
462 landslide areas suggests that even as the frequency of large storm events in the Kosñipata Valley  
463 decreases, the landslide area associated with these events may increase commensurately, such that the  
464 effects compensate.

465 We can further explore the amount of work done, again in terms of landslide area, by the cumulative  
466 effect of repeated events of small magnitude versus occasional events of larger magnitude. We  
467 calculate the % work done for a year with a given recurrence interval as  $W_i = (A_i/\Sigma A)/RI_i \times 100$ ,  
468 where  $A_i$  is the landslide area in year  $i$  and  $\Sigma A$  is the total landslide area in the full dataset. When  $W_i$  is  
469 plotted versus  $RI_i$ , the compensating effect of frequency and magnitude is evident (Fig. 3c). With the  
470 exception of the most frequent years that are characterized by very little landslide activity (low  $RI$  and  
471 low  $W$ ), most years are characterized by a fairly similar value of  $W$ . Thus we expect that the long-  
472 term total landslide area resulting from years characterized by storm activity of varying magnitude is,  
473 on average, very similar in this setting. In other words, the landslide work done in years with rare,  
474 large storms is more or less similar to the sum of the total integrated work done in those years with  
475 smaller but more frequent storms.

476 Many previous studies of storm-triggered landslides have focused specifically on storm events (e.g.,  
477 Wohl and Ogden, 2013; Ramos Scharrón et al., 2012; West et al., 2011) and lacked such longer-term  
478 context, although several studies on storm triggers of landslides have been concerned with identifying  
479 threshold storm intensities for failure (e.g., Guzzetti et al., 2007; Glade, 1998; Larsen and Simon,  
480 1993). Time series with higher temporal resolution associated with individual storm events of varying  
481 magnitude rather than annual total landslide areas as used in this study would provide a test of the  
482 inferences made here, and analyses similar to that in this study for storm-triggered landslides in other  
483 settings would help shed more light on how storms contribute to erosional processes in mountain  
484 landscapes. Nonetheless, even though the total work done by large magnitude storms may not exceed  
485 that done by smaller events over the long term, the immediacy of large storm effects may be  
486 important from the perspectives of hazards, fluvial impacts, and biogeochemical processes. For  
487 example, large events will supply large amounts of clastic sediment (Wang et al., 2015) and organic  
488 material (West et al., 2011) in a short space of time.

## 489 **5.2. Spatial patterns of landslide activity**

### 490 **5.2.1 Spatial patterns and their relation to the 2010 storm**

491 Spatial and temporal patterns of landslides depend on proximal triggers such as rainfall and seismic  
492 activity (Lin et al., 2008; Meunier et al., 2008; Densmore and Hovius, 2000), as well as on  
493 geomorphic pre-conditions, such as bedrock strength and slope angle, the latter of which is at least in  
494 part regulated by fluvial incision by rivers (Larsen and Montgomery, 2012; Bussmann et al., 2008;  
495 Lin et al., 2008). The observation of highest landslide susceptibility in the Kosñipata Valley at highest  
496 slopes in the catchment reflects the importance of slope angle for landslide failure. The notable shift  
497 from low to high landslide susceptibility above 30-40° (Fig. 6b) is consistent with the hillslope angles  
498 that reflect rock strength expected for the metamorphic and plutonic bedrock (Larsen and  
499 Montgomery, 2012). Generally, the greater overall landslide susceptibility at the lower elevations in  
500 the Kosñipata Valley is consistent with the higher slope angles at these elevations (Figs. 2, 5, 10b).  
501 This set of observations is consistent with predictions of a threshold hillslope model (cf. Gallen et al.,  
502 2015; Roering et al., 2015; Larsen and Montgomery, 2012).

503 In more detail, the distribution of landslides with respect to elevation in the Kosñipata Valley is  
504 complicated by clustering of the 2010 storm-triggered landslides at low elevations. This clustering  
505 may be explained at least in part by the focused intensity of the 2010 storm precipitation at low  
506 elevations; much lower rainfall was recorded on March 4<sup>th</sup> at a meteorology station at 2900 m  
507 elevation in the Kosñipata Valley (at the Wayqecha forest plot), compared to the San Pedro  
508 meteorological station at 1450 m elevation (Fig. 9a). Although the single 2010 event may not  
509 contribute more to the development of long-term landslide area than the cumulative effect of smaller  
510 events (see above), the landslides from this one specific event do significantly influence the overall  
511 spatial distribution of landslides visible in present-day imagery. One implication of this observation is  
512 that landslide maps based on all visible landslides at any one point in time, assuming uniform rates of  
513 occurrence, may overlook the role of specific proximal triggering events that lead to spatial clustering.  
514 Such event-clustering may influence inferred relationships between landslides and controlling factors  
515 such as regional precipitation gradients or patterns of uplift, emphasizing that time-sequence of  
516 landslide occurrence may be important to accurately assessing such relationships.

### 517 **5.2.2 Storm triggered landslides at low elevations: Stochastic happenstance or characteristic of** 518 **long-term erosional patterns?**

519 The elevation distribution of landslides in the 2010 storm is clearly distinct from the background  
520 landslide activity during the 25-year study period. This difference raises an important question: are the  
521 2010 landslides representative of a distinct spatial pattern associated with larger storm events? Or are  
522 the spatial locations of these landslides reflective of one stochastic storm event that happened to be  
523 captured in our analysis and is part of a series of events that shift in location throughout the catchment  
524 over time? We cannot distinguish these possibilities conclusively, but we do have some evidence that



525 allows for preliminary inferences that could be tested with further work. Two lines of evidence  
526 suggest that the focusing of storm-triggered landslides at low elevations in the Kosñipata study  
527 catchment may be characteristic of long-term spatial patterns in which routine landslides occur  
528 throughout the catchment while rarer, intense landslide events selectively affect the lower elevations.

529 The first line of evidence is that the magnitude-frequency statistics for precipitation indicate that low-  
530 frequency events of high-magnitude (i.e., relatively infrequent but large storms) are more  
531 characteristic at low elevation sites compared to high elevations (Fig. 9b). This statistical tendency  
532 toward more storm activity at low elevations would provide a mechanism for regular storm-triggering  
533 of landslides at these elevations.

534 A second set of information comes from the Kosñipata Valley topography and its relation to implied  
535 erosion associated with landslide activity. Although total landslide area in our Kosñipata dataset is  
536 greatest at mid-elevations, these mid-elevation landslides are distributed over a relatively large  
537 catchment area (Fig. 5a). Effective landslide erosion is greatest where landslide susceptibility on a  
538 unit-area basis is highest (Fig. 5b), so our inventory implies focused landslide erosion at lower  
539 elevations (<~1500-2000 m) in the Kosñipata Valley, specifically associated with the 2010 storm  
540 (Figs. 2a, 5). This focused erosion appears to spatially coincide with the observed transition in the  
541 river channel profile at ~1700 m elevation, marked by the vertical step knickpoint (Fig. 10a). In the  
542 Kosñipata Valley, this transition occurs near a lithological change from sedimentary to plutonic  
543 bedrock. However, as best known the lithological contact does not exactly coincide spatially with the  
544 knickpoint, and the other principal rivers in the region are also characterised by similar transitions in  
545 channel morphology even though they do not have the same lithological transition, suggesting that  
546 lithology is not the primary control on the observed transition in channel morphology (Fig. 11).

547 Several other processes can generate knickpoints in river profiles (e.g., Whipple, 2001). The  
548 topographic transition in the Kosñipata and in neighbouring catchments appears to approximately  
549 coincide with changes in precipitation regime, and specifically with less cloud cover and greater storm  
550 occurrence below the level of most persistent annual cloud cover in the Andean mid-elevations. (cf.  
551 Espinoza et al., 2015 and Rohrmann et al., 2014 for the southern central Andes). By increasing  
552 erosional efficiency, this climatic transition may at least in part contribute to generating the observed  
553 channel profile. Other effects may also be important, for example the transient upstream propagation  
554 of erosion driven by past changes in uplift, as proposed for the eastern Andes in Bolivia (Whipple and  
555 Gasparini, 2014), or unidentified geologic structures in the Alto Madre de Dios region. These  
556 possibilities are discussed further below.

557 Whatever the underlying cause, hillslope angles downstream of the transitions in channel morphology  
558 are generally steeper than those upstream (Figs. 10b and 11c), consistent with the downstream slopes  
559 being more prone to landslide failure over the long term. The total area of landslides triggered on low-

560 elevation slopes in 2010 does not exceed the accumulated landslide area in the rest of the catchment  
561 over the longer term (see discussion of magnitude-frequency above, and histograms of landslide area  
562 in Fig. 5a). Nonetheless, these low-elevation landslides are concentrated in a smaller area (Fig. 5b)  
563 and therefore represent higher landslide susceptibility, greater rates of landscape lowering and more  
564 frequent hillslope turnover.

565 Based on the consistency of catchment topography with the landslide distribution that includes 2010  
566 storm-triggered landslides, we speculate that the high rates of landslide erosion at low elevations in  
567 the Kosñipata catchment are characteristic of long-term erosional patterns. This hypothesis could be  
568 tested by complementing the landslide analysis presented in this study with measurements of long-  
569 term denudation rates in small tributary basins of the Kosñipata Valley above and below the apparent  
570 morphologic transition. Although we acknowledge that we currently lack such supporting  
571 independent evidence, in the following sections we include consideration of some of the possible  
572 implications of our hypothesized transition towards higher landslide occurrence at lower elevations in  
573 the Kosñipata Valley.

### 574 **5.3. Landslide-driven erosion and regional topography**

575 In general terms, high-elevation, low-slope surfaces, such as those that characterize the upper portions  
576 of the Kosñipata Valley, are thought to have a number of possible origins, including (i) the uplift and  
577 preservation of previously low-lying “relict” surfaces (e.g., Clark et al., 2006), (ii) glacial “buzz-saw”  
578 levelling of surfaces near the glacial equilibrium line altitude (Brozović et al., 1997), (iii) erosion of  
579 rocks with contrasting strength (e.g., Oskin and Burbank, 2005), and (iv) in situ generation through  
580 river system reorganization over time (Yang et al., 2015). There is no evidence for a glacial or  
581 lithological cause for low-relief parts of the Kosñipata Valley and the immediately adjacent portions  
582 of the Andean plateau, suggesting either a relict origin or in situ fluvial formation. Similar high-  
583 elevation, low-relief surfaces south of our study region, along the eastern flank of the Andes in  
584 Bolivia, have been proposed as relict landscapes uplifted in the past ~10-12 Myrs (Whipple and  
585 Gasparini, 2014; Barke and Lamb, 2006; Gubbels et al., 1993). By this interpretation, erosion into the  
586 eastern Andean margins has generated escarpments but not yet erased the original surfaces (Whipple  
587 and Gasparini, 2014).

588 From landslide mapping in the Kosñipata Valley, we infer higher hillslope erosion rates at lower  
589 elevations and particularly downstream of the knickpoint in this catchment. Even when ignoring the  
590 very low-elevation landslides associated with the 2010 storm in our dataset, the occurrence of  
591 landslides throughout the 25-year study period are notably shifted to lower elevations compared to the  
592 Kosñipata catchment area (Fig. 5c). This pattern emphasizes that erosion rates are low at the highest  
593 elevations, where slopes are also lower presumably because incision is less pronounced. If our  
594 observed landslide rates reflect long-term erosion, these observations are consistent with the idea that

595 the low slopes at high elevations in this region of the Andes are preserved because propagation of  
596 more rapid erosion at low elevations has not yet reached the low-slope parts of the landscape. But,  
597 based on the distribution of landslide erosion alone, we cannot distinguish whether the low slope  
598 regions have their origin as relict landscapes or features resulting from fluvial reorganization.

599 The importance of storm triggering for setting the spatial patterns of landslide activity in the  
600 Kosñipata Valley suggests that greater storm frequency (e.g., Fig. 9b) could be an important  
601 mechanism facilitating higher erosion rates at low elevations in this catchment, consistent with  
602 climate variability being a major erosional driver (DiBiase and Whipple, 2011; Lague et al., 2005).  
603 The indication of a mechanistic link between precipitation patterns and erosion in the Kosñipata  
604 catchment may provide clues about how climatic gradients leave an imprint on the topography of the  
605 eastern Andes (e.g., Strecker et al., 2007), potentially superimposed on tectonically-controlled  
606 patterns of transient erosion into the uplifted mountain range (Gasparini and Whipple, 2014).  
607 Although previous studies have considered the role of gradients in precipitation magnitude across  
608 strike of the eastern Andes (e.g., Gasparini and Whipple, 2014; Lowman and Barros, 2014)), we note  
609 that little work has considered the role of storm frequency, which our analysis suggests may be  
610 variable and important in setting erosion patterns in this region.

611 Based on our landslide dataset and the precipitation statistics for the Kosñipata Valley, we speculate  
612 that the greater precipitation magnitude and frequency of large storm events below the cloud  
613 immersion zone in the eastern Andes of the Madre de Dios basin work to facilitate a combination of  
614 hillslope failure, sediment removal, and river channel incision. Channel incision, facilitated by high  
615 storm runoff and the tools provided by landslide erosion (e.g., Crosby et al., 2007), increases hillslope  
616 angles, and landslide failure keeps pace, triggered by storm events such as the 2010 event observed in  
617 our dataset. Focused, climatically controlled erosion at lower elevations along the eastern flank of the  
618 Andes in the Madre de Dios basin could contribute to the preservation of relatively low-slope surfaces  
619 at high elevations: if rates of erosion in and above the cloud immersion zone are limited by decreased  
620 precipitation and particularly reduced storm frequency, the upstream propagation of erosion may be  
621 inhibited, reducing the potential for rivers to incise into the low slope regions in the high-elevation  
622 headwaters. This, in turn, may explain why rivers along the eastern flank of the Andes in Peru have  
623 not succeeded in eroding back into the Andean topography sufficiently to “capture” the flow of the  
624 Altiplano rivers (e.g., the tributaries of the Rio Urubamba that currently flow several hundred  
625 kilometres to the north via the Ucayali before cutting east through the Andes to join the Amazonas).  
626 Our results thus raise the possibility of a potential climatic mechanism for sustaining this topographic  
627 contrast and prolonging the persistence of the asymmetric morphology in this region of the Andes.

#### 628 **5.4. Landslide transfer of organic carbon to rivers**

629 The  $26 \pm 4 \text{ tC km}^{-2} \text{ yr}^{-1}$  of organic carbon stripped from hillslope soil and vegetation during our study  
630 period reflects a significant catchment-scale carbon transfer (Stallard, 1998). The area-normalized  
631 landslide carbon yield in the Kosñipata Valley is similar to the upper end of values for other mountain  
632 sites around the world where analogous carbon fluxes have been evaluated. For example, in a region  
633 of Guatemala with a 20-year hurricane return time, landslide carbon yields were  $33 \text{ tC km}^{-2} \text{ yr}^{-1}$   
634 (Ramos Scharrón et al., 2012), similar to our Kosñipata results. In the western Southern Alps of New  
635 Zealand, landslide carbon yields were  $17 \pm 6 \text{ tC km}^{-2} \text{ yr}^{-1}$  in catchments where landslide rates were  
636 highest, while the mean yield was much lower, at  $\sim 8 \text{ tC km}^{-2} \text{ yr}^{-1}$  (Hilton et al., 2011). In part, the high  
637 carbon flux we observe in the Kosñipata Valley reflects the high organic carbon stocks of soils in this  
638 catchment ( $27\,680 \pm 4\,420 \text{ tC km}^{-2}$ ), larger than the mean estimated in the western Southern Alps,  
639 New Zealand ( $18\,000 \pm 9\,000 \text{ tC km}^{-2}$ ; Hilton et al., 2011). The high flux can also be attributed to the  
640 high rates of landsliding driven by the combination of steep topography and intense precipitation  
641 events (and presumably on multi-centennial timescales by large earthquakes).

642 Following the recolonization of landslide scars (Fig. 8), the fate of landslide-derived organic carbon  
643 governs whether erosion acts as a source or sink of carbon dioxide to the atmosphere (Ramos  
644 Scharrón et al., 2012; Hilton et al., 2011). Bedrock landslides may supply organic carbon to rivers at  
645 the same point in time and space as large amounts of clastic sediment are delivered from hillslopes  
646 (Hilton et al., 2011; Hovius et al., 1997). The association of organic matter with high mineral loads  
647 enhances its potential for sedimentary burial and longer-term sequestration of atmospheric carbon  
648 dioxide (Galy et al., 2015; Hilton et al., 2011). In contrast, oxidation of biospheric organic carbon  
649 eroded by landslides represents a poorly quantified source of  $\text{CO}_2$  for assessments of ecosystem  
650 carbon balance.

651 The extent to which landslides connect to river channels exerts a first-order control on the fate of  
652 landslide material (Dadson et al., 2004), and thus on the fate of carbon. We identified landslides as  
653 connected or unconnected to rivers by manually inspecting high-resolution imagery and following  
654 landslides to their termination (i.e. to their lowest elevation point). Connected landslides terminated in  
655 river channels, identifiable by the absence of vegetation. We found that, for the Kosñipata Valley  
656 during our study period, greater than 90% of landslides were directly connected with rivers, similar to  
657 the high connectivity found for other storm-triggered landslides (e.g., West et al., 2011). However,  
658 even with high connectivity, it remains uncertain in the case of the Kosñipata how much of the  
659 material stripped by landslides is actually removed by rivers and exported out of the valley.

660 While quantifying the onward fluvial transfer of organic carbon stripped by landslides and its fate in  
661 the Madre de Dios River and wider Amazon Basin is out of the scope of the present study, our  
662 observations provide baseline data for interpreting river flux measurements, as well as important new  
663 insight on the role of landslides in the routing of organic carbon in mountain catchments. First, we

664 note that the location of landslides within a catchment may influence whether the organic material  
665 eroded from hillslopes is transported by rivers (Hilton et al., 2008b). The observation that landslide  
666 erosion may be non-uniform thus has important implications for organic carbon fate. In lower-order  
667 streams, landslides may be less likely to connect to rivers (Ramos Scharrón et al., 2012), and rivers  
668 are less likely to have capacity to export material, compared to higher order streams. In the Kosñipata  
669 River, focused erosion of organic carbon occurs in the low/mid-elevations and is likely to act to  
670 enhance delivery into higher order river channels, optimizing the potential for removal from the river  
671 catchment. For instance, the mid-elevations (2100 m to 3000 m) are the source of the majority (51%)  
672 of the organic material (in terms of mass per time) eroded from hillslopes by landslides, because these  
673 elevations cover the greatest proportion of total basin area (43%) (Fig. 12a). On a per-area basis (i.e.,  
674 in  $\text{tC km}^{-2} \text{yr}^{-1}$ ), landslide mobilisation of organic carbon is most frequent at lower elevations (Fig.  
675 12b); while the land area in the Kosñipata study area below 1800 m elevation comprises 9% of the  
676 total catchment area, 18% of the organic material stripped by landslides comes from these elevations  
677 (Figs. 12a, 12b).

678 Second, the landslide-derived organic carbon yield is mostly (80%) derived from soil organic matter.  
679 This material is finer-grained than coarse woody debris and is thus more likely to be entrained and  
680 transported by the Kosñipata River. This observation is consistent with measurements of the isotopic  
681 and elemental composition of river-borne particulate organic carbon (POC) in this catchment, which  
682 suggest that soil organic carbon from upper horizons appears to be a significant source of biospheric  
683 POC (Clark et al., 2013). While the total POC export fluxes from the Kosñipata River are still to be  
684 quantified, it is likely that the landslide process offers a mechanism by which large quantities of  
685 organic matter, and particularly fine-grained soil organic matter susceptible to fluvial transport, can be  
686 supplied from steep hillslopes to river channels.

687 Finally, our observations are important for understanding the episodic delivery of Andean-derived  
688 organic matter to river systems via the landslide process. The distinct focusing of 2010 rain storm-  
689 driven erosion at low elevations of the Kosñipata study catchment demonstrates the potential for  
690 landslides triggered by individual storm events to erode material selectively from within a  
691 catchment's elevation range. Measurements of biomarker isotope composition in downstream river  
692 sediment have shown that organic erosional products reflect distinct elevation sources during storms  
693 (Ponton et al., 2014). Together, these results emphasize the potential role for storm events to  
694 determine the organic biomarker composition delivered to sediments and to introduce biases relative  
695 to the uniform catchment integration often assumed of erosion (Bouchez et al., 2014; Ponton et al.,  
696 2014).

697 **5.5. Timescales of re-vegetation and implications for ecosystem disturbance and composition**

698 The biomass and soil removed by landslides is regenerated on hillslopes over time. The duration and  
699 dynamics of vegetation recovery influence vegetation structure and soil structure, provide habitat for  
700 various species, play an integral role in nutrient cycling, and determine the timescale over which  
701 standing stocks of organic carbon are replenished (Restrepo et al., 2009; Bussmann et al., 2008). For  
702 the Kosñipata study catchment, we estimate that 100% of the landslide area from a given year reaches  
703 full vegetation cover that is indistinguishable from the surrounding vegetation (based on observable  
704 changes from 1988 to 2011 in remote sensing imagery) at  $\sim 27 \pm 8$  yrs after landslide occurrence (Fig.  
705 8). Individual landslides showed large variability; one landslide with a very large area at high  
706 elevation, visible in an air photo from 1963, is still visible with active portions in 2011, indicating that  
707 at least portions of very large landslides may take longer ( $>48$  yrs) to revegetate, partly due to  
708 reactivation. On the other hand, the shortest revegetation time for a landslide occurred within 4 years.  
709 In the Bolivian Andes, at sites with similar montane forest and similar elevation range, similar  
710 revegetation times of 10 to 35 yrs were estimated based on dating trees on landslide scars and  
711 evaluating canopy closure in aerial photographs (Blodgett and Isacks, 2007).

712 Although the return to vegetation cover on landslide scars may occur over several decades, it may  
713 take much longer, perhaps hundreds of years, to reach the full maturity of a tropical montane cloud  
714 forest and to fully replenish soil carbon stocks (Walker et al., 1996). Post-landslide vegetation  
715 modelling in the Ecuadorian Andes (1900-2100 m) suggested that initial return of vegetation to  
716 landslide surfaces occurs within 80 years after a landslide but that it takes at least 200 years for the  
717 post-landslide forest to develop the biomass of a mature tropical montane forest (Dislich and Huth,  
718 2012). The timescale of this full maturation process may be important when considering the impact of  
719 landslides on carbon budgets and ecosystem dynamics.

720 Repeated cycles of landslide activity and re-vegetation have the potential to introduce disturbance to  
721 ecosystems that may affect soil nutrient status, carbon stocks, and even plant biodiversity (Restrepo et  
722 al., 2009). Patches of bare rock left by landslides undergo ‘quasi-primary’ succession (Restrepo et al.,  
723 2009) that promotes movement of organisms and ecosystem reorganisation (Walker et al., 2013;  
724 Hupp, 1983), while inhibiting ecosystem retrogression and nutrient depletion (Peltzer et al., 2010). On  
725 landslides in the Bolivian Andes, plant species richness increased from early to late succession and  
726 then declined in very mature or senescent forests (Kessler, 1999).

727 In the Kosñipata Valley, the spatial trends in landslide rate with elevation are similar to trends in plant  
728 species richness measured at forest plots (Fig. 13). Similar to landslide activity, species richness is  
729 lowest at high elevations, increases slightly with decreasing elevation to 2000 m, and then increases  
730 abruptly (from 80 to 180 species  $\text{ha}^{-1}$ ) on forested hillslopes between 2000 m and  $\sim 1700$  m (Fig. 13).  
731 The coincidence of these patterns may reflect the control of both landslides and biodiversity by  
732 climatic conditions (e.g., both greater landslide activity and greater biodiversity below the cloud

733 immersion zone). Or the patterns may be simply coincidental, with biodiversity regulated by factors  
734 independent of landslide erosion, such as light and temperature, or the transition between  
735 lowland/submontane species and montane cloud forest species. We suggest that it may also be  
736 possible that the intermediate disturbance regime (Connell, 1978) associated with landslide activity at  
737 the lower catchment elevations influences ecosystem structure (Walker et al., 2013; Restrepo et al.,  
738 2009; Kessler, 1999; Hupp, 1983) and contributes to enhanced biodiversity observed below ~1700 m.  
739 Such effects could be consistent with peaks in species richness at mid-elevations (around 1500 m)  
740 observed across Andean forest plots in Peru (Fig. 13), Bolivia, and Ecuador (Engemann et al., 2015;  
741 Salazar et al., 2015; Girardin et al., 2014b; Huaraca Huasco et al., 2014). A complex mix of  
742 geomorphic, climatic and ecological factors likely influence landslide and biodiversity patterns, but  
743 coincidence in our dataset provides impetus for future studies of species diversity along  
744 geomorphically-imposed gradients of disturbance.

745

## 746 **7. Conclusions**

747 We have quantified the spatial and temporal patterns of landslides over 25-years in the Kosñipata  
748 Valley, a forested mountain catchment in the Peruvian Andes. Over the 25 year period, one extreme  
749 rainfall event in 2010 triggered ~1/4 of all inventoried landslides, demonstrating the importance of  
750 large rainfall events for landslide activity in the Andes. The annual data from this study suggest that  
751 the cumulative landslide area associated with smaller, more frequent storms may be similar to the area  
752 associated with larger, rarer storms.

753 The landslides mobilized significant amounts of carbon from forested hillslopes, with an average  
754 yield of  $26 \pm 4 \text{ tC km}^{-2} \text{ yr}^{-1}$ . This is one of the largest erosive fluxes of biospheric carbon recorded in a  
755 mountain catchment. We estimate that a large proportion of this material was from soil organic matter  
756 ( $20 \pm 3 \text{ tC km}^{-2} \text{ yr}^{-1}$ ) scoured from depths of ~1.5m or less, with above- and below-ground biomass  
757 marking a smaller, yet still important contribution ( $5.7 \pm 0.8 \text{ tC km}^{-2} \text{ yr}^{-1}$ ). That coupled with the  
758 observation that ~90% of the mapped landslide areas were spatially connected to river channels  
759 suggests that this biospheric carbon may be very mobile, and may contribute importantly to suspended  
760 sediment export by the Kosñipata River. The onward fate of this carbon will play an important role in  
761 determining whether landsliding and physical erosion processes in the Andes contributes a net carbon  
762 dioxide source or sink.

763 Landslides observed in this study were not distributed uniformly across the catchment area, but were  
764 focused on slopes above a threshold angle (ca. 30-40°), consistent with previous studies and  
765 theoretical expectations. The highest elevations in the catchment are characterized by low slopes and  
766 relatively little landslide activity. Landslides triggered by the large storm in 2010 cluster at low  
767 elevations, where precipitation magnitude-frequency relations and catchment morphology hint that

768 such pulses of intense erosional activity may be characteristic of long-term patterns. Such non-  
769 uniform erosion would have implications for sources and composition of sediment, organic matter and  
770 associated biomarkers and could potentially contribute to influencing forest species composition  
771 through patterns of disturbance. Relations between storm activity, landsliding and landscape processes  
772 and ecological function merit further investigation to probe these possible links.

773



774 **Appendix A. High-resolution Digital Elevation Model**

775 For analysing the topography of the Kosñipata study catchment, we used a DEM generated from the  
776 Carnegie Airborne Observatory 2 (CAO-2) next generation Airborne Taxonomic Mapping System  
777 (AToMS) with an Airborne Light Detection and Ranging (LiDAR) (Asner et al., 2012). The CAO  
778 data was processed to 1.12 m spot spacing. Laser ranges from the LiDAR were combined with the  
779 embedded high resolution Global Positioning System-Inertial Measurement Unit (GPS-IMU) data to  
780 determine the 3-D locations of laser returns, producing a ‘cloud’ of LiDAR data. The LiDAR data  
781 cloud consists of a very large number of georeferenced point elevation estimates (cm), where  
782 elevation is relative to a reference ellipsoid (WGS 1984). To estimate canopy height above ground,  
783 LiDAR data points were processed to identify which laser pulses penetrated the canopy volume and  
784 reached the ground surface. We used these points to interpolate a raster digital terrain model (DTM)  
785 for the ground surface. This was achieved using a 10 m x 10 m kernel passed over each flight block;  
786 the lowest elevation estimate in each kernel was assumed to be ground. Subsequent points were  
787 evaluated by fitting a horizontal plane to each of the ground seed points. If the closest unclassified  
788 point was  $< 5.5^\circ$  and  $< 1.5$  m higher in elevation, it was classified as ground. This process was  
789 repeated until all points within the block were evaluated. The cell resolution was derived from the  
790 DEM resampled in ArcGIS to a 3 m x 3 m DEM to smooth the topography from a 1.12 m x 1.12 m  
791 DEM. Cells in the topographic shadow area and the area of the catchment with a gap in the data ( $\sim 3$   
792 km<sup>2</sup> centralised in the upper elevations) were removed from this analysis.

793

794 *Author contributions.* K. E. Clark, A. J. West, R. G. Hilton, Y. Malhi, M. New, M. R. Silman, and S.  
795 S. Saatchi designed the study; G. P. Asner and R. E. Martin carried out Carnegie Airborne  
796 Observatory (CAO) data acquisition and analysis; C. A. Quesada carried out the soil stock fieldwork  
797 and geochemical analysis; W. Farfan-Rios and M. R. Silman carried out the above ground living  
798 biomass and plant species diversity fieldwork; A. B. Horwath carried out the bryophyte carbon stock  
799 fieldwork; K. Halladay carried out the MODIS cloud cover analysis; K. E. Clark carried the analysis  
800 under the advisement of A. J. West and with contributions from Y. Malhi and R. G. Hilton. K. E.  
801 Clark and A. J. West prepared the manuscript with contributions from all of the co-authors.

802

803

#### 804 **Acknowledgements**

805 This paper is a product of the Andes Biodiversity and Ecosystems Research Group (ABERG). KEC  
806 was funded by the Natural Sciences and Engineering Research Council of Canada (NSERC) and  
807 Clarendon Fund PhD scholarships. AJW was supported to work in the Kosñipata Valley by NSF-EAR  
808 1227192 and RGH was supported by a NERC New Investigator Grant (NE/I001719/1). YM is  
809 supported by the Jackson Foundation and a European Research Council Advanced Investigator Grant  
810 GEM-TRAIT. The Carnegie Airborne Observatory is made possible by the Avatar Alliance  
811 Foundation, Grantham Foundation for the Protection of the Environment, John D. and Catherine T.  
812 MacArthur Foundation, Gordon and Betty Moore Foundation, W. M. Keck Foundation, Margaret A.  
813 Cargill Foundation, Mary Anne Nyburg Baker and G. Leonard Baker Jr., and William R. Hearst III.  
814 We thank D. Knapp, T. Kennedy-Bowdoin, C. Anderson, and R. Tupayachi for CAO data collection  
815 and analysis; M. Palace for the QuickBird-2 satellite images from 2009 and 2010; S. Abele for GIS  
816 advice; S. Moon and G. Hilley for providing Matlab code for slope-area analysis; and S. Feakins and  
817 reviewers of a prior submission for comments. We thank Ken Ferrier and an anonymous referee for  
818 their helpful and insightful reviews.

819

820

821 **References**

- 822 ACCA: Weather data San Pedro station, Asociación para la conservación de la cuenca Amazónica  
 823 <http://atrium.andesamazon.org/index.php>, (accessed 01/04/2012), 2012.
- 824 Asner, G. P., Powell, G. V., Mascaro, J., Knapp, D. E., Clark, J. K., Jacobson, J., Kennedy-Bowdoin, T.,  
 825 Balaji, A., Paez-Acosta, G., and Victoria, E.: High-resolution forest carbon stocks and  
 826 emissions in the Amazon, *P Natl. Acad. Sci. USA*, 107, 16738-16742,  
 827 10.1073/pnas.1004875107, 2010.
- 828 Asner, G. P., Knapp, D. E., Boardman, J., Green, R. O., Kennedy-Bowdoin, T., Eastwood, M., Martin, R.  
 829 E., Anderson, C., and Field, C. B.: Carnegie Airborne Observatory-2: Increasing science data  
 830 dimensionality via high-fidelity multi-sensor fusion, *Remote Sens. Environ.*, 124, 454-465,  
 831 10.1016/j.rse.2012.06.012, 2012.
- 832 Asner, G. P., Knapp, D. E., Martin, R. E., Tupayachi, R., Anderson, C. B., Mascaro, J., Sinca, F.,  
 833 Chadwick, K. D., Higgins, M., Farfan, W., Llactayo, W., and Silman, M. R.: Targeted carbon  
 834 conservation at national scales with high-resolution monitoring, *P. Natl. Acad. Sci. USA*, 111,  
 835 E5016-E5022, 10.1073/pnas.1419550111, 2014.
- 836 Barke, R., and Lamb, S.: Late Cenozoic uplift of the Eastern Cordillera, Bolivian Andes, *Earth Planet*  
 837 *Sc. Lett.*, 249, 350-367, 10.1016/j.epsl.2006.07.012, 2006.
- 838 Bilderback, E. L., Pettinga, J. R., Litchfield, N. J., Quigley, M., Marden, M., Roering, J. J., and Palmer, A.  
 839 S.: Hillslope response to climate-modulated river incision in the Waipaoa catchment, East  
 840 Coast North Island, New Zealand, *Geol. Soc. Am. Bull.*, 127, 131-148, 10.1130/B31015.1,  
 841 2015.
- 842 Blodgett, T. A., and Isacks, B. L.: Landslide erosion rate in the eastern cordillera of northern Bolivia,  
 843 *Earth Interact.*, 11, 1-30, 10.1175/2007EI222.1, 2007.
- 844 Bookhagen, B.: High resolution spatiotemporal distribution of rainfall seasonality and extreme  
 845 events based on a 12-year TRMM time series  
 846 <http://www.geog.ucsb.edu/~bodo/TRMM/index.php>, (accessed 06/06/2013), 2013.
- 847 Bouchez, J., Galy, V., Hilton, R. G., Gaillardet, J., Moreira-Turcq, P., Pérez, M. A., France-Lanord, C.,  
 848 and Maurice, L.: Source, transport and fluxes of Amazon River particulate organic carbon:  
 849 insights from river sediment depth-profiles, *Geochim. Cosmochim. Ac.*, 133, 280-298,  
 850 10.1016/j.gca.2014.02.032, 2014.
- 851 Brozović, N., Burbank, D. W., and Meigs, A. J.: Climatic limits on landscape development in the  
 852 Northwestern Himalaya, *Science*, 276, 571-574, 10.1126/science.276.5312.571, 1997.
- 853 Burbank, D. W., Leland, J., Fielding, E., Anderson, R. S., Brozovic, N., Reid, M. R., and Duncan, C.:  
 854 Bedrock incision, rock uplift and threshold hillslopes in the northwestern Himalayas, *Nature*,  
 855 379, 505-510, 10.1038/379505a0, 1996.
- 856 Bussmann, R. W., Wilcke, W., and Richter, M.: Landslides as important disturbance regimes - Causes  
 857 and regeneration, in: *Gradients in a tropical mountain ecosystem of Ecuador*, edited by:  
 858 Beck, E., Bendix, J., Kottke, I., Makeschin, F., and Mosandl, R., *Ecological Studies*, 198,  
 859 Springer-Verlag, Berlin Heidelberg, Germany, 321-330, 2008.
- 860 Cabrera, J., Sébrier, M., and Mercier, J. L.: Plio-Quaternary geodynamic evolution of a segment of the  
 861 Peruvian Andean Cordillera located above the change in the subduction geometry: The  
 862 Cuzco region, *Tectonophysics*, 190, 331-362, 10.1016/0040-1951(91)90437-W, 1991.
- 863 Carlotto Caillaux, V. S., Rodriguez, G., Fernando, W., Roque, C., Dionicio, J., and Chávez, R.: *Geología*  
 864 *de los cuadrángulos de Urubamba y Calca*, Instituto Geológica Nacional, Lima, Peru, 1996.
- 865 Casagli, N., Dapporto, S., Ibsen, M. L., Tofani, V., and Vannocci, P.: Analysis of the landslide triggering  
 866 mechanism during the storm of 20th–21st November 2000, in *Northern Tuscany, Landslides*,  
 867 3, 13-21, 10.1007/s10346-005-0007-y, 2006.
- 868 Clark, K. E., Hilton, R. G., West, A. J., Malhi, Y., Gröcke, D. R., Bryant, C. L., Ascough, P. L., Robles  
 869 Caceres, A., and New, M.: New views on “old” carbon in the Amazon River: Insight from the

870 source of organic carbon eroded from the Peruvian Andes, *Geochem. Geophys. Geosy.*, 14,  
871 1644-1659, 10.1002/ggge.20122, 2013.

872 Clark, K. E., Torres, M. A., West, A. J., Hilton, R. G., New, M., Horwath, A. B., Fisher, J. B., Rapp, J. M.,  
873 Robles Caceres, A., and Malhi, Y.: The hydrological regime of a forested tropical Andean  
874 catchment, *Hydrol. Earth Syst. Sci.*, 18, 5377-5397, 10.5194/hess-18-5377-2014, 2014.

875 Clark, M. K., Royden, L. H., Whipple, K. X., Burchfiel, B. C., Zhang, X., and Tang, W.: Use of a regional,  
876 relict landscape to measure vertical deformation of the eastern Tibetan Plateau, *J. Geophys.*  
877 *Res.-Earth*, 111, 1-23, 10.1029/2005JF000294, 2006.

878 Connell, J. H.: Diversity in tropical rain forests and coral reefs, *Science*, 199, 1302-1310,  
879 10.1126/science.199.4335.1302, 1978.

880 Consbio: Ecosistemas Terrestres de Peru (Data Basin Dataset) for ArcGIS, Covallis, Oregon, USA,  
881 2011.

882 Crosby, B. T., Whipple, K. X., Gasparini, N. M., and Wobus, C. W.: Formation of fluvial hanging  
883 valleys: Theory and simulation, *J. Geophys. Res.-Earth*, 112, 1-20, 10.1029/2006JF000566,  
884 2007.

885 Dadson, S. J., Hovius, N., Chen, H., Dade, W. B., Lin, J.-C., Hsu, M.-L., Lin, C.-W., Horng, M.-J., Chen, T.-  
886 C., Milliman, J., and Stark, C. P.: Earthquake-triggered increase in sediment delivery from an  
887 active mountain belt, *Geology*, 32, 733-736, 10.1130/G20639.1 2004.

888 Densmore, A. L., and Hovius, N.: Topographic fingerprints of bedrock landslides, *Geology*, 28, 371-  
889 374, 10.1130/0091-7613(2000)28<371:TFOBL>2.0.CO;2 2000.

890 DiBiase, R. A., and Whipple, K. X.: The influence of erosion thresholds and runoff variability on the  
891 relationships among topography, climate, and erosion rate, *J. Geophys. Res.-Earth*, 116, 1-  
892 17, 10.1029/2011JF002095, 2011.

893 Dislich, C., and Huth, A.: Modelling the impact of shallow landslides on forest structure in tropical  
894 montane forests, *Ecol. Model.*, 239, 40-53, 10.1016/j.ecolmodel.2012.04.016, 2012.

895 Dixon, R. K., Brown, S., Houghton, R., Solomon, A., Trexler, M., and Wisniewski, J.: Carbon pools and  
896 flux of global forest ecosystems, *Science*, 263, 185-189, 1994.

897 Egholm, D. L., Knudsen, M. F., and Sandiford, M.: Lifespan of mountain ranges scaled by feedbacks  
898 between landsliding and erosion by rivers, *Nature*, 498, 475-478, 10.1038/nature12218,  
899 2013.

900 Ekström, G., and Stark, C. P.: Simple scaling of catastrophic landslide dynamics, *Science*, 339, 1416-  
901 1419, 10.1126/science.1232887, 2013.

902 Engemann, K., Enquist, B. J., Sandel, B., Boyle, B., Jørgensen, P. M., Morueta-Holme, N., Peet, R. K.,  
903 Violle, C., and Svenning, J.-C.: Limited sampling hampers "big data" estimation of species  
904 richness in a tropical biodiversity hotspot, *Ecol. Evol.*, 5, 807-820, 10.1002/ece3.1405, 2015.

905 Espinoza, J. C., Chavez, S., Ronchail, J., Junquas, C., Takahashi, K., and Lavado, W.: Rainfall hotspots  
906 over the southern tropical Andes: Spatial distribution, rainfall intensity, and relations with  
907 large-scale atmospheric circulation, *Water Resour. Res.*, 51, 1-17, 10.1002/2014WR016273,  
908 2015.

909 Eswaran, H., Van Den Berg, E., and Reich, P.: Organic Carbon in Soils of the World, *Soil Sci. Soc. Am.*  
910 *J.*, 57, 192-194, 10.2136/sssaj1993.03615995005700010034x, 1993.

911 Farr, T. G., Rosen, P. A., Caro, E., Crippen, R., Duren, R., Hensley, S., Kobrick, M., Paller, M.,  
912 Rodriguez, E., Roth, L., Seal, D., Shaffer, S., Shimada, J., Umland, J., Werner, M., Oskin, M.,  
913 Burbank, D., and Alsdorf, D.: The Shuttle Radar Topography Mission, *Rev. Geophys.*, 45,  
914 RG2004, 10.1029/2005RG000183, 2007.

915 Ferrier, K. L., Huppert, K. L., and Perron, J. T.: Climatic control of bedrock river incision, *Nature*, 496,  
916 206-209, 10.1038/nature11982, 2013.

917 Gallen, S. F., Clark, M. K., and Godt, J. W.: Coseismic landslides reveal near-surface rock strength in a  
918 high-relief tectonically active setting, *Geology*, 43, 70-70, 10.1130/G36080.1 2015.

919 Galy, V., Peucker-Ehrenbrink, B., and Eglinton, T.: Global carbon export from the terrestrial  
920 biosphere controlled by erosion, *Nature*, 521, 204-207, 10.1038/nature14400, 2015.

921 Gasparini, N. M., and Whipple, K. X.: Diagnosing climatic and tectonic controls on topography:  
922 Eastern flank of the northern Bolivian Andes, *Lithosphere*, 6, 230-250, 10.1130/l322.1, 2014.

923 Gibbon, A., Silman, M. R., Malhi, Y., Fisher, J. B., Meir, P., Zimmermann, M., Dargie, G. C., Farfan, W.  
924 R., and Garcia, K. C.: Ecosystem carbon storage across the grassland-forest transition in the  
925 high Andes of Manu National Park, Peru, *Ecosystems*, 13, 1097-1111, 10.1007/s10021-010-  
926 9376-8, 2010.

927 Gilbert, G. K.: *Geology of the Henry Mountains*, Geology of the Henry Mountains, Washington, D.C.,  
928 Report, i-160 pp., 1877.

929 Girardin, C. A. J., Malhi, Y., Aragao, L. E. O. C., Mamani, M., Huasco, W. H., Durand, L., Feeley, K. J.,  
930 Rapp, J., Silva-Espejo, J. E., Silman, M., Salinas, N., and Whittaker, R. J.: Net primary  
931 productivity allocation and cycling of carbon along a tropical forest elevational transect in  
932 the Peruvian Andes, *Glob. Change Biol.*, 16, 3176-3192, 10.1111/j.1365-2486.2010.02235.x,  
933 2010.

934 Girardin, C. A. J., Aragão, L. E. O. C., Malhi, Y., Huaraca Huasco, W., Metcalfe, D. B., Durand, L.,  
935 Mamani, M., Silva-Espejo, J. E., and Whittaker, R. J.: Fine root dynamics along an elevational  
936 gradient in tropical Amazonian and Andean forests, *Global Biogeochem. Cy.*, 27, 252-264,  
937 10.1029/2011GB004082, 2013.

938 Girardin, C. A. J., Malhi, Y., Feeley, K. J., Rapp, J. M., Silman, M. R., Meir, P., Huaraca Huasco, W.,  
939 Salinas, N., Mamani, M., Silva-Espejo, J. E., García Cabrera, K., Farfan Rios, W., Metcalfe, D.  
940 B., Doughty, C. E., and Aragão, L. E. O. C.: Seasonality of above-ground net primary  
941 productivity along an Andean altitudinal transect in Peru, *J. Trop. Ecol.*, 30, 503-519,  
942 10.1017/S0266467414000443, 2014a.

943 Girardin, C. A. J., Silva-Espejo, J. E., Doughty, C. E., Huaraca Huasco, W., Metcalfe, D. B., Durand-Baca,  
944 L., Marthews, T. R., Aragao, L. E. O. C., Farfan Rios, W., García Cabrera, K., Halladay, K.,  
945 Fisher, J. B., Galiano-Cabrera, D. F., Huaraca-Quispe, L. P., Alzamora-Taype, I., Equiluz-Mora,  
946 L., Salinas-Revilla, N., Silman, M., Meir, P., and Malhi, Y.: Productivity and carbon allocation  
947 in a tropical montane cloud forest of the Peruvian Andes, *Plant Ecol. Divers.*, 7, 107-123,  
948 10.1080/17550874.2013.820222, 2014b.

949 Glade, T.: Establishing the frequency and magnitude of landslide-triggering rainstorm events in New  
950 Zealand, *Eng. Geol.*, 35, 160-174, 10.1007/s002540050302, 1998.

951 Gregory-Wodzicki, K. M.: Uplift history of the Central and Northern Andes: A review, *Geol. Soc. Am.*  
952 *Bull.*, 112, 1091-1105, 10.1130/0016-7606(2000)112<1091:UHOTCA>2.0.CO;2 2000.

953 Gubbels, T. L., Isacks, B. L., and Farrar, E.: High-level surfaces, plateau uplift, and foreland  
954 development, Bolivian central Andes, *Geology*, 21, 695-698, 10.1130/0091-  
955 7613(1993)021<0695:hlsqua>2.3.co;2, 1993.

956 Gurdak, D. J., Aragao, L. E. O. C., Rozas-Dávila, A., Huaraca Huasco, W., García Cabrera, K., Doughty,  
957 C. E., Farfan-Rios, W., Silva-Espejo, J. E., Metcalfe, D. B., Silman, M. R., and Malhi, Y.:  
958 Assessing above-ground woody debris dynamics along a gradient of elevation in Amazonian  
959 cloud forests in Peru: balancing above-ground inputs and respiration outputs, *Plant Ecol.*  
960 *Divers.*, 7, 143-160, 10.1080/17550874.2013.818073, 2014.

961 Guzzetti, F., Peruccacci, S., Rossi, M., and Stark, C. P.: Rainfall thresholds for the initiation of  
962 landslides in central and southern Europe, *Meteorol. Atmos. Phys.*, 98, 239-267,  
963 10.1007/s00703-007-0262-7, 2007.

964 Halladay, K., Malhi, Y., and New, M.: Cloud frequency climatology at the Andes/Amazon transition: 1.  
965 Seasonal and diurnal cycles, *J. Geophys. Res.*, 117, D23102, 10.1029/2012JD017770, 2012.

966 Hilton, R. G., Galy, A., and Hovius, N.: Riverine particulate organic carbon from an active mountain  
967 belt: Importance of landslides, *Global Biogeochem. Cy.*, 22, BG1017,  
968 10.1029/2006GB002905, 2008a.

969 Hilton, R. G., Galy, A., Hovius, N., Chen, M.-C., Horng, M.-J., and Chen, H.: Tropical-cyclone-driven  
970 erosion of the terrestrial biosphere from mountains, *Nat Geosci*, 1, 759-762,  
971 10.1038/ngeo333, 2008b.

972 Hilton, R. G., Meunier, P., Hovius, N., Bellingham, P. J., and Galy, A.: Landslide impact on organic  
973 carbon cycling in a temperate montane forest, *Earth Surf. Proc. Land.*, 36, 1670-1679,  
974 10.1002/esp.2191, 2011.

975 Hilton, R. G., Gaillardet, J., Calmels, D., and Birck, J.-L.: Geological respiration of a mountain belt  
976 revealed by the trace element rhenium, *Earth Planet Sc. Lett.*, 403, 27-36,  
977 10.1016/j.epsl.2014.06.021, 2014.

978 Horwath, A.: Epiphytic bryophytes as cloud forest indicators: Stable isotopes, biomass and diversity  
979 along an altitudinal gradient in Peru, Doctor of Philosophy, Plant Sciences, University of  
980 Cambridge, Cambridge, 260 pp., 2011.

981 Hovius, N., Stark, C. P., and Allen, P. A.: Sediment flux from a mountain belt derived by landslide  
982 mapping, *Geology*, 25, 231-234, 10.1130/0091-7613(1997)025<0231:sffamb>2.3.co;2, 1997.

983 Hovius, N., Stark, C. P., Chu, H. T., and Lin, J. C.: Supply and removal of sediment in a landslide-  
984 dominated mountain belt: Central Range, Taiwan, *J. Geol.*, 108, 73-89, 10.1086/314387,  
985 2000.

986 Huaraca Huasco, W., Girardin, C. A. J., Doughty, C. E., Metcalfe, D. B., Baca, L. D., Silva-Espejo, J. E.,  
987 Cabrera, D. G., Aragão, L. E. O., Davila, A. R., Marthews, T. R., Huaraca-Quispe, L. P.,  
988 Alzamora-Taype, I., Eguiluz-Mora, L., Farfan-Rios, W., Cabrera, K. G., Halladay, K., Salinas-  
989 Revilla, N., Silman, M., Meir, P., and Malhi, Y.: Seasonal production, allocation and cycling of  
990 carbon in two mid-elevation tropical montane forest plots in the Peruvian Andes, *Plant Ecol.*  
991 *Divers.*, 1-2, 125-142, 10.1080/17550874.2013.819042, 2014.

992 Hupp, C. R.: Seedling establishment on a landslide site, *Castanea*, 48, 89-98, 1983.

993 INGEMMET: GEOCATMIN - Geologia integrada por proyectos regionales, Lima, Peru, 2013.

994 Keefer, D. K.: The importance of earthquake-induced landslides to long-term slope erosion and  
995 slope-failure hazards in seismically active regions, *Geomorphology*, 10, 265-284,  
996 10.1016/0169-555X(94)90021-3, 1994.

997 Kessler, M.: Plant species richness and endemism during natural landslide succession in a perhumid  
998 montane forest in the Bolivian Andes, *Ecotropica*, 5, 123-136, 1999.

999 Lague, D., Hovius, N., and Davy, P.: Discharge, discharge variability, and the bedrock channel profile,  
1000 *J. Geophys. Res.-Earth*, 110, 1-17, 10.1029/2004JF000259, 2005.

1001 Larsen, I. J., Montgomery, D. R., and Korup, O.: Landslide erosion controlled by hillslope material,  
1002 *Nat. Geosci.*, 3, 247-251, 10.1038/ngeo776, 2010.

1003 Larsen, I. J., and Montgomery, D. R.: Landslide erosion coupled to tectonics and river incision, *Nat.*  
1004 *Geosci.*, 5, 468-473, 10.1038/ngeo1479, 2012.

1005 Larsen, M. C., and Simon, A.: A rainfall intensity-duration threshold for landslides in a humid-tropical  
1006 environment, Puerto Rico, *Geogr. Ann. A.*, 75, 13-23, 10.2307/521049, 1993.

1007 Li, G., West, A. J., Densmore, A. L., Jin, Z., Parker, R. N., and Hilton, R. G.: Seismic mountain building:  
1008 Landslides associated with the 2008 Wenchuan earthquake in the context of a generalized  
1009 model for earthquake volume balance, *Geochem. Geophys. Geosy.*, 15, 833-844,  
1010 10.1002/2013GC005067, 2014.

1011 Lin, G.-W., Chen, H., Hovius, N., Horng, M.-J., Dadson, S., Meunier, P., and Lines, M.: Effects of  
1012 earthquake and cyclone sequencing on landsliding and fluvial sediment transfer in a  
1013 mountain catchment, *Earth Surf. Proc. Land.*, 33, 1354-1373, 10.1002/esp.1716, 2008.

1014 Lowman, L. E. L., and Barros, A. P.: Investigating links between climate and orography in the Central  
1015 Andes: Coupling erosion and precipitation using a physical-statistical model, *J. Geophys.*  
1016 *Res.-Earth*, 119, 1322-1353, 10.1002/2013JF002940, 2014.

1017 Malamud, B. D., Turcotte, D. L., Guzzetti, F., and Reichenbach, P.: Landslide inventories and their  
1018 statistical properties, *Earth Surf. Proc. Land.*, 29, 687-711, 10.1002/esp.1064, 2004.

1019 Malhi, Y., Silman, M., Salinas, N., Bush, M., Meir, P., and Saatchi, S.: Introduction: Elevation gradients  
1020 in the tropics: Laboratories for ecosystem ecology and global change research, *Glob. Change*  
1021 *Biol.*, 16, 3171-3175, 10.1111/j.1365-2486.2010.02323.x, 2010.

1022 Marc, O., and Hovius, N.: Amalgamation in landslide maps: effects and automatic detection, *Nat.*  
1023 *Hazards Earth Syst. Sci.*, 15, 723-733, 10.5194/nhess-15-723-2015, 2015.

1024 Marengo, J. A., Soares, W. R., Saulo, C., and Nicolini, M.: Climatology of the low-level jet east of the  
1025 Andes as derived from the NCEP-NCAR reanalyses: Characteristics and temporal variability, *J.*  
1026 *Climate*, 17, 2261-2280, 10.1175/1520-0442(2004)017<2261:COTLJE>2.0.CO;2, 2004.

1027 Marvin, D. C., Asner, G. P., Knapp, D. E., Anderson, C. B., Martin, R. E., Sinca, F., and Tupayachi, R.:  
1028 Amazonian landscapes and the bias in field studies of forest structure and biomass, *P. Natl.*  
1029 *Acad. Sci. USA*, 111, E5224-E5232, 10.1073/pnas.1412999111, 2014.

1030 Mendivil Echevarría, S., and Dávila Manrique, D.: *Geología de los cuadrángulos de Cuzco y Livitaca*,  
1031 Instituto Geológica Nacional, Lima, Peru, 1994.

1032 METI/NASA: ASTER Global DEM product, NASA EOSDIS Land Processes DAAC USGS Earth Resources  
1033 Observation and Science (EROS) Center Sioux Falls, South Dakota, USA, 2009.

1034 Meunier, P., Hovius, N., and Haines, J. A.: Topographic site effects and the location of earthquake  
1035 induced landslides, *Earth Planet Sc. Lett.*, 275, 221-232, 10.1016/j.epsl.2008.07.020, 2008.

1036 Montgomery, D. R., and Buffington, J. M.: Channel-reach morphology in mountain drainage basins,  
1037 *Geol. Soc. Am. Bull.*, 109, 596-611, 10.1130/0016-7606(1997)109<0596:CRMIMD>2.3.CO;2,  
1038 1997.

1039 Montgomery, D. R.: Slope distributions, threshold hillslopes, and steady-state topography, *Am. J.*  
1040 *Sci.*, 301, 432-454, 10.2475/ajs.301.4-5.432, 2001.

1041 Montgomery, D. R., and Brandon, M. T.: Topographic controls on erosion rates in tectonically active  
1042 mountain ranges, *Earth Planet Sc. Lett.*, 201, 481-489, 10.1016/S0012-821X(02)00725-2,  
1043 2002.

1044 Moon, S., Chamberlain, C. P., Blisniuk, K., Levine, D. H., Rood, D. H., and Hilley, G. E.: Climatic control  
1045 of denudation in the deglaciated landscape of the Washington Cascades, *Nat. Geosci.*, 4,  
1046 469-473, 10.1038/ngeo1159, 2011.

1047 Oskin, M., and Burbank, D. W.: Alpine landscape evolution dominated by cirque retreat, *Geology*, 33,  
1048 933-936, 10.1130/G21957.1, 2005.

1049 Peltzer, D. A., Wardle, D. A., Allison, V. J., Baisden, W. T., Bardgett, R. D., Chadwick, O. A., Condon, L.  
1050 M., Parfitt, R. L., Porder, S., and Richardson, S. J.: Understanding ecosystem retrogression,  
1051 *Ecol. Mongr.*, 80, 509-529, 10.1890/09-1552.1, 2010.

1052 Pepin, E., Guyot, J. L., Armijos, E., Bazan, H., Fraizy, P., Moquet, J. S., Noriega, L., Lavado, W.,  
1053 Pombosa, R., and Vauchel, P.: Climatic control on eastern Andean denudation rates (Central  
1054 Cordillera from Ecuador to Bolivia), *J. S. Am. Earth Sci.*, 44, 85-93,  
1055 10.1016/j.jsames.2012.12.010, 2013.

1056 Ponton, C., West, A. J., Feakins, S. J., and Galy, V.: Leaf wax biomarkers in transit record river  
1057 catchment composition, *Geophys. Res. Lett.*, 41, 6420-6427, 10.1002/2014GL061328, 2014.

1058 Quesada, C. A., Lloyd, J., Schwarz, M., Patiño, S., Baker, T. R., Czimczik, C., Fyllas, N. M., Martinelli, L.,  
1059 Nardoto, G. B., Schmerler, J., Santos, A. J. B., Hodnett, M. G., Herrera, R., Luizão, F. J., Arneeth,  
1060 A., Lloyd, G., Dezzio, N., Hilke, I., Kuhlmann, I., Raessler, M., Brand, W. A., Geilmann, H.,  
1061 Moraes Filho, J. O., Carvalho, F. P., Araujo Filho, R. N., Chaves, J. E., Cruz Junior, O. F.,  
1062 Pimentel, T. P., and Paiva, R.: Variations in chemical and physical properties of Amazon  
1063 forest soils in relation to their genesis, *Biogeosciences*, 5, 1515 - 1541, 10.5194/bg-7-1515-  
1064 2010, 2010.

1065 Raich, J. W., Russell, A. E., Kitayama, K., Parton, W. J., and Vitousek, P. M.: Temperature influences  
1066 carbon accumulation in moist tropical forests, *Ecology*, 87, 76-87, 10.1890/05-0023, 2006.

1067 Ramos Scharrón, C. E., Castellanos, E. J., and Restrepo, C.: The transfer of modern organic carbon by  
1068 landslide activity in tropical montane ecosystems, *J. Geophys. Res.-Biogeo.*, 117, G03016,  
1069 10.1029/2011JG001838, 2012.

1070 Rao, Y.: Variation in plant carbon and nitrogen isotopes along an altitudinal gradient in the Peruvian  
1071 Andes, *B.Sc.*, Department of Earth Sciences, Durham University, Durham, 60 pp., 2011.

1072 Restrepo, C., Vitousek, P., and Neville, P.: Landslides significantly alter land cover and the  
1073 distribution of biomass: an example from the Ninole ridges of Hawai'i, *Plant Ecol.*, 166, 131-  
1074 143, 10.1023/A:1023225419111, 2003.

1075 Restrepo, C., and Alvarez, N.: Landslides and their contribution to land-cover change in the  
1076 mountains of Mexico and Central America, *Biotropica*, 38, 446-457, 10.1111/j.1744-  
1077 7429.2006.00178.x, 2006.

1078 Restrepo, C., Walker, L. R., Shiels, A. B., Bussmann, R., Claessens, L., Fisch, S., Lozano, P., Negi, G.,  
1079 Paolini, L., and Poveda, G.: Landsliding and its multiscale influence on mountainscapes,  
1080 *Bioscience*, 59, 685-698, 10.1525/bio.2009.59.8.10, 2009.

1081 Roering, J. J., Kirchner, J. W., and Dietrich, W. E.: Characterizing structural and lithologic controls on  
1082 deep-seated landsliding: Implications for topographic relief and landscape evolution in the  
1083 Oregon Coast Range, USA, *Geol. Soc. Am. Bull.*, 117, 654-668, 10.1130/B25567.1, 2005.

1084 Roering, J. J., Mackey, B. H., Handwerger, A. L., Booth, A. M., Schmidt, D. A., Bennett, G. L., and  
1085 Cerovski-Darriau, C.: Beyond the angle of repose: A review and synthesis of landslide  
1086 processes in response to rapid uplift, Eel River, Northern California, *Geomorphology*, 236,  
1087 109-131, 10.1016/j.geomorph.2015.02.013, 2015.

1088 Rohrmann, A., Strecker, M. R., Bookhagen, B., Mulch, A., Sachse, D., Pingel, H., Alonso, R. N.,  
1089 Schildgen, T. F., and Montero, C.: Can stable isotopes ride out the storms? The role of  
1090 convection for water isotopes in models, records, and paleoaltimetry studies in the central  
1091 Andes, *Earth Planet Sc. Lett.*, 407, 187-195, 10.1016/j.epsl.2014.09.021, 2014.

1092 Saatchi, S. S., Houghton, R. A., Dos Santos Alvalá, R. C., Soares, J. V., and Yu, Y.: Distribution of  
1093 aboveground live biomass in the Amazon basin, *Glob. Change Biol.*, 13, 816-837,  
1094 10.1111/j.1365-2486.2007.01323.x, 2007.

1095 Saatchi, S. S., Harris, N. L., Brown, S., Lefsky, M., Mitchard, E. T., Salas, W., Zutta, B. R., Buermann,  
1096 W., Lewis, S. L., and Hagen, S.: Benchmark map of forest carbon stocks in tropical regions  
1097 across three continents, *P. Natl. Acad. Sci. USA*, 108, 9899-9904, 10.1073/pnas.1019576108,  
1098 2011.

1099 Safran, E. B., Bierman, P. R., Aalto, R., Dunne, T., Whipple, K. X., and Caffee, M.: Erosion rates driven  
1100 by channel network incision in the Bolivian Andes, *Earth Surf. Proc. Land.*, 30, 1007-1024,  
1101 10.1002/esp.1259, 2005.

1102 Salazar, L., Homeier, J., Kessler, M., Abrahamczyk, S., Lehnert, M., Krömer, T., and Kluge, J.: Diversity  
1103 patterns of ferns along elevational gradients in Andean tropical forests, *Plant Ecol. Divers.*, 8,  
1104 13-24, 10.1080/17550874.2013.843036, 2015.

1105 Schmidt, K. M., and Montgomery, D. R.: Limits to relief, *Science*, 270, 617-620,  
1106 10.1126/science.270.5236.617, 1995.

1107 Sébrier, M., Mercier, J. L., Mégard, F., Laubacher, G., and Carey-Gailhardis, E.: Quaternary normal  
1108 and reverse faulting and the state of stress in the central Andes of south Peru, *Tectonics*, 4,  
1109 739-780, 10.1029/TC004i007p00739, 1985.

1110 Selby, M.: *Hillslope materials and processes*, Oxford University Press, Oxford, UK, 289 pp., 1993.

1111 Stallard, R. F.: River chemistry, geology, geomorphology, and soils in the Amazon and Orinoco Basins,  
1112 *The chemistry of weathering*, Rodez, France, 293-316, 1985.

1113 Stallard, R. F.: Terrestrial sedimentation and the carbon cycle: Coupling weathering and erosion to  
1114 carbon burial, *Global Biogeochem. Cy.*, 12, 231-257, 10.1029/98gb00741, 1998.

1115 Stark, C. P., and Hovius, N.: The characterization of landslide size distributions, *Geophys. Res. Lett.*,  
1116 28, 1091-1094, 10.1029/2000GL008527, 2001.

1117 Stock, J., and Dietrich, W. E.: Valley incision by debris flows: Evidence of a topographic signature,  
1118 *Water Resour. Res.*, 39, 1-24, 10.1029/2001WR001057, 2003.

1119 Stoyan, R.: *Aktivität, Ursachen und Klassifikation der Rutschungen in San Francisco/Süd Ecuador*,  
1120 *Diploma*, University of Erlangen-Nuremberg, Erlangen, Germany, 2000.



1121 Strecker, M. R., Alonso, R. N., Bookhagen, B., Carrapa, B., Hilley, G. E., Sobel, E. R., and Trauth, M. H.:  
1122 Tectonics and climate of the Southern Central Andes, *Annu. Rev. Earth Pl. Sc.*, 35, 747-787,  
1123 10.1146/annurev.earth.35.031306.140158, 2007.

1124 Tavera, H., and Buforn, E.: Source mechanism of earthquakes in Perú, *J. Seismol.*, 5, 519-540,  
1125 10.1023/A:1012027430555, 2001.

1126 Terzaghi, K.: Mechanism of landslides, Harvard University, Department of Engineering, Cambridge,  
1127 Massachusetts, USA, 41 pp., 1951.

1128 USGS: Earthquakes v3.6, 2013-07-02, USGS, <http://earthquake.usgs.gov/earthquakes/map/>, access:  
1129 02/07/2013, 2013a.

1130 USGS: Landsat Processing Details, United States Geological Survey, U.S. Department of the Interior,  
1131 [http://landsat.usgs.gov/Landsat\\_Processing\\_Details.php](http://landsat.usgs.gov/Landsat_Processing_Details.php), access: 16/7/2013, 2013b.

1132 Vargas Vilchez, L., and Hipolito Romero, A.: Geología de los cuadrángulos de Río Piquén, Pilcopata y  
1133 Chontachaca. Hojas: 25-t, 26-t y 27-t, Instituto Geológica Nacional, Lima, Peru, 1998.

1134 Walker, L. R., Zarin, D. J., Fetcher, N., Myster, R. W., and Johnson, A. H.: Ecosystem development and  
1135 plant succession on landslides in the Caribbean, *Biotropica*, 28, 566-576, 10.2307/2389097,  
1136 1996.

1137 Walker, L. R., Shiels, A. B., Bellingham, P. J., Sparrow, A. D., Fetcher, N., Landau, F. H., and Lodge, D.  
1138 J.: Changes in abiotic influences on seed plants and ferns during 18 years of primary  
1139 succession on Puerto Rican landslides, *J. Ecol.*, 101, 650-661, 10.1111/1365-2745.12071,  
1140 2013.

1141 Wang, G., and Sassa, K.: Pore-pressure generation and movement of rainfall-induced landslides:  
1142 effects of grain size and fine-particle content, *Eng. Geol.*, 69, 109-125, 10.1016/S0013-  
1143 7952(02)00268-5, 2003.

1144 Wang, J., Jin, Z., Hilton, R. G., Zhang, F., Densmore, A. L., Li, G., and West, A. J.: Controls on fluvial  
1145 evacuation of sediment from earthquake-triggered landslides, *Geology*, 43, 115-118,  
1146 10.1130/G36157.1, 2015.

1147 West, A. J., Lin, C. W., Lin, T. C., Hilton, R. G., Liu, S. H., Chang, C. T., Lin, K. C., Galy, A., Sparkes, R. B.,  
1148 and Hovius, N.: Mobilization and transport of coarse woody debris to the oceans triggered  
1149 by an extreme tropical storm, *Limnol. Oceanogr.*, 56, 77-85, 10.4319/lo.2011.56.1.0077,  
1150 2011.

1151 Whipple, K. X.: Fluvial landscape response time: How plausible is steady-state denudation?, *Am. J.*  
1152 *Sci.*, 301, 313-325, 10.2475/ajs.301.4-5.313, 2001.

1153 Whipple, K. X.: Bedrock rivers and the geomorphology of active orogens, *Annu. Rev. Earth Pl. Sc.*, 32,  
1154 151-185, 10.1146/annurev.earth.32.101802.120356, 2004.

1155 Whipple, K. X., and Gasparini, N. M.: Tectonic control of topography, rainfall patterns, and erosion  
1156 during rapid post-12 Ma uplift of the Bolivian Andes, *Lithosphere*, 6, 251-268,  
1157 10.1130/l325.1, 2014.

1158 Wittmann, H., von Blanckenburg, F., Guyot, J. L., Maurice, L., and Kubik, P.: From source to sink:  
1159 Preserving the cosmogenic <sup>10</sup>Be-derived denudation rate signal of the Bolivian Andes in  
1160 sediment of the Beni and Mamoré foreland basins, *Earth Planet Sc. Lett.*, 288, 463-474,  
1161 10.1016/j.epsl.2009.10.008, 2009.

1162 Wohl, E., and Ogden, F. L.: Organic carbon export in the form of wood during an extreme tropical  
1163 storm, Upper Rio Chagres, Panama, *Earth Surf. Proc. Land.*, 38, 1407-1416,  
1164 10.1002/esp.3389, 2013.

1165 Wolman, M. G., and Miller, J. P.: Magnitude and frequency of forces in geomorphic processes, *J.*  
1166 *Geol.*, 68, 54-74, 1960.

1167 Yang, R., Willett, S. D., and Goren, L.: In situ low-relief landscape formation as a result of river  
1168 network disruption, *Nature*, 520, 526-529, 10.1038/nature14354, 2015.

1169 Yoo, K., Amundson, R., Heimsath, A. M., and Dietrich, W. E.: Erosion of upland hillslope soil organic  
1170 carbon: Coupling field measurements with a sediment transport model, *Global Biogeochem.*  
1171 *Cy.*, 19, GB3003, 10.1029/2004GB002271, 2005.

1172 Zhang, W., and Montgomery, D. R.: Digital elevation model grid size, landscape representation,  
1173 Water Resour. Res., 30, 1019-1028, 1994.

1174 Zimmermann, M., Meir, P., Bird, M. I., Malhi, Y., and Ccahuana, A. J. Q.: Climate dependence of  
1175 heterotrophic soil respiration from a soil-translocation experiment along a 3000 m tropical  
1176 forest altitudinal gradient, Eur. J. Soil Sci., 60, 895-906, 10.1111/j.1365-2389.2009.01175.x,  
1177 2009.

1178

1179

1180

Table 1: Regressions for basin wide carbon stocks (tC km <sup>-2</sup> ) for the Kosñipata Valley				
Equation	Number of plots	R <sup>2</sup>	P	Source of data
Soil = 4.01±4.64 x Elevation + 16665.22±11753.06	11 (with 6 to 51 subplots)	0.08	0.19	This study
AGLB = -1.16±0.65 x Elevation + 8553.71±1644.36	13	0.22	0.10	This study
BGLB = -0.22±0.13 x Elevation + 2237.09±280.18	6	0.43	0.16	(Girardin et al., 2010)
AGLB = Above ground living biomass (includes tree stems)				
BGLB = Below ground living biomass (includes fine and coarse roots)				
Regressions used to gain a general understanding of C stocks with elevation and significance of the relationship with elevation is not relevant.				

1181

1182

1183

Table 2: Valley-wide landslide stripped organic carbon ( $\text{tC km}^{-2} \text{yr}^{-1}$ ).

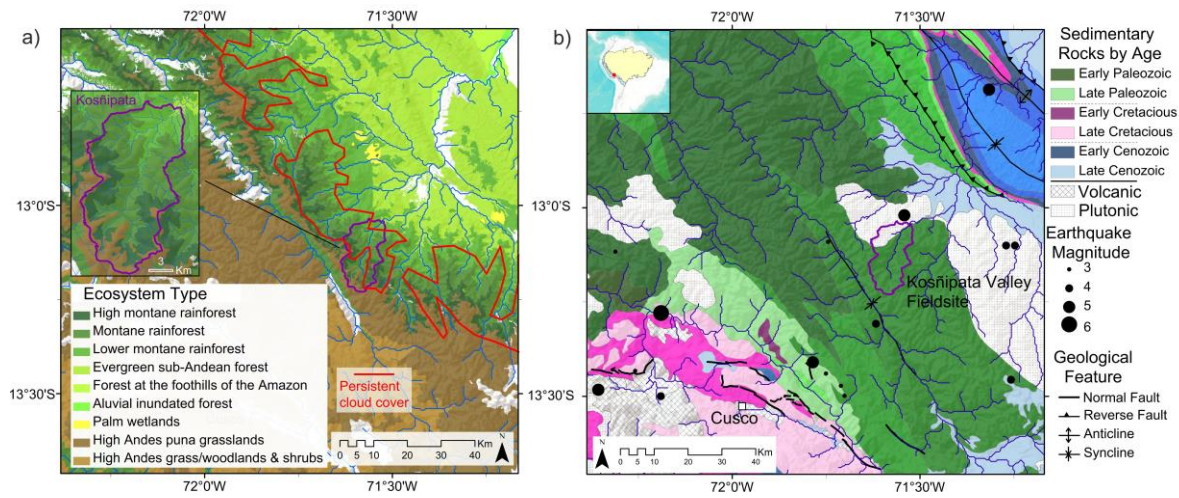
	1988 to 2012	Without 2010	2010
Total	$25.8 \pm 3.6$	$19.1 \pm 3.0$	$6.8 \pm 1.2$
Soil	$20.1 \pm 3.5$	$15.1 \pm 2.9$	$5.0 \pm 1.2$
Vegetation	$5.7 \pm 0.8$	$4.0 \pm 0.7$	$1.7 \pm 0.2$

1184

1185

1186  
1187

## Figures

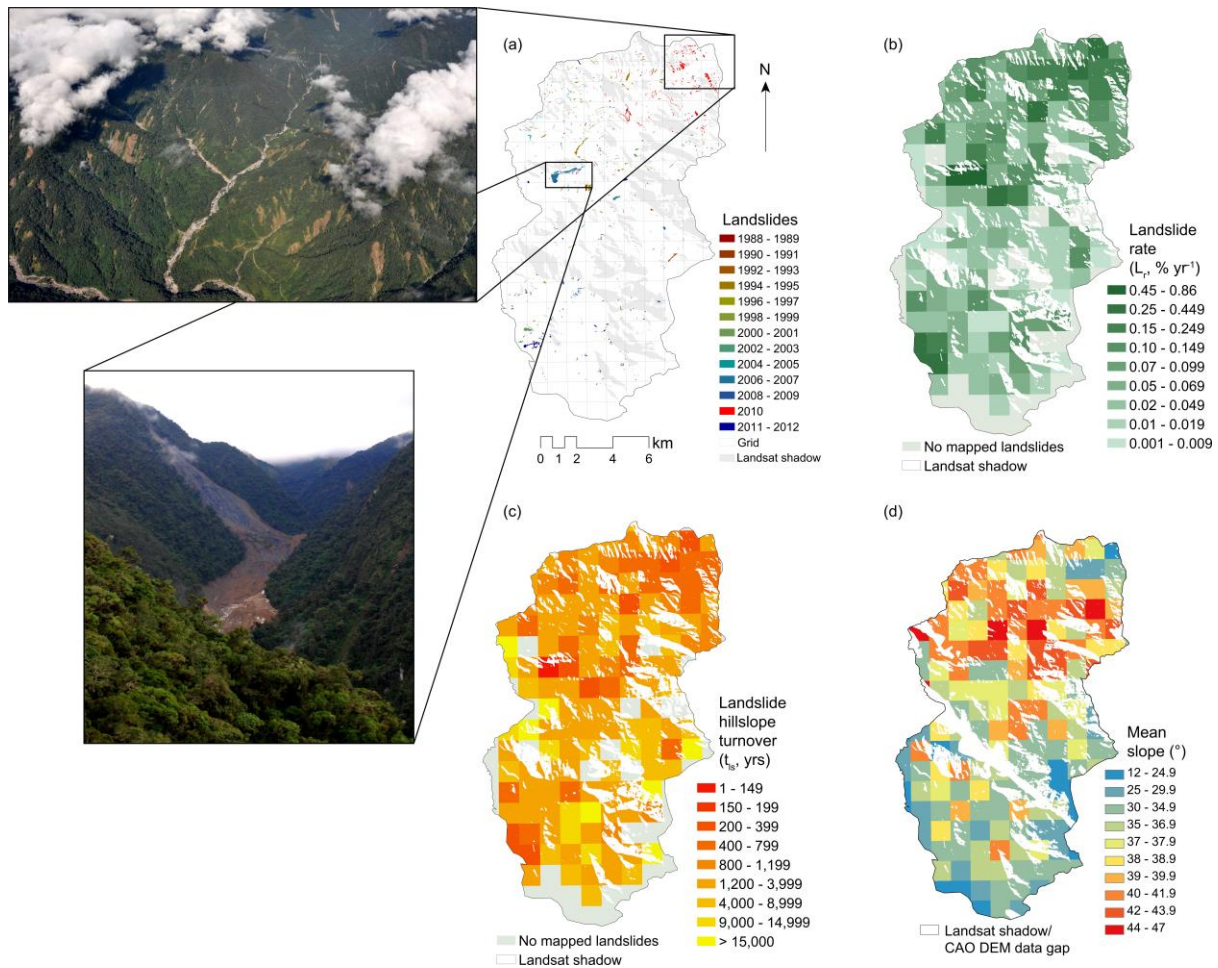


1188

1189 Figure 1: Maps of the study region. (a) Ecosystem types in the eastern Andes of Peru (Consbio, 2011).  
1190 Bare areas are cities, agriculture, glaciers and riverbed, with the Kosñipata study catchment magnified  
1191 in the inset. Areas delimited by red polygons are regions of > 75% annual cloud cover (Halladay et  
1192 al., 2012). (b) Georectified geological map (INGEMMET, 2013; Vargas Vilchez and Hipolito  
1193 Romero, 1998; Carlotto Caillaux et al., 1996; Mendivil Echevarría and Dávila Manrique, 1994);  
1194 sedimentary rocks are on a scale ranging from dark to light colour within each era. Active faults  
1195 (Cabrera et al., 1991; Sébrier et al., 1985) and documented earthquakes since 1975 (USGS, 2013a) are  
1196 shown.

1197

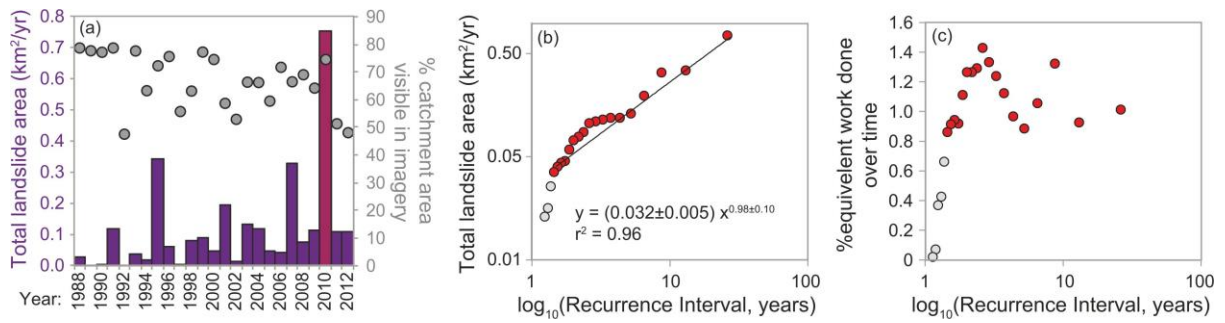
1198



1199

1200 Figure 2: (a) Landslides over the 25-year study period mapped from Landsat satellite images with  
 1201 annual resolution, with Landsat topographic shadow regions in light grey. Photographs of the 2010  
 1202 landslides (upper) taken by Gregory P. Asner from the Carnegie Airbone Observatory (CAO) in 2013,  
 1203 and of the largest landslide in the study in 2007 (lower) taken by William Farfan-Rios from the  
 1204 ground in 2011. (b) Landslide rates ( $R_{ls}$ , % yr<sup>-1</sup>) calculated by 1 km<sup>2</sup> grid cell. (c) Hillslope turnover  
 1205 ( $t_{ls}$ , yr) rates calculated as the time for landslides, at the current measured rate ( $R_{ls}$ ), to impact 100% of  
 1206 each cell area. (d) Catchment slopes calculated over a 1 km<sup>2</sup> grid for the visible portion of the study  
 1207 area using the CAO DEM with 3m x 3m resolution.

1208

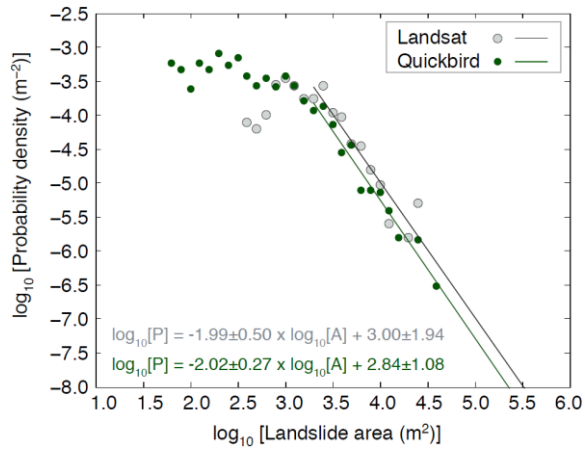


1209

1210 Figure 3: (a) Total area of landslides occurring each year in the dataset from this study, along with the  
 1211 % area visible in the images used for each year. (b) Magnitude-frequency relationship for landslide  
 1212 areas mapped in each year; red points are included in the regression while grey point are excluded  
 1213 since these lowest-magnitude years depart from the linear relationship. (c) Estimate of integrated  
 1214 work done by repeated events characteristic of given return times (see main text). Landslide area  
 1215 mapped in 2010 was significantly higher than any other year because of landslides triggered by the  
 1216 large storm in March 2010, but above a threshold magnitude, the integrated long-term landslide area  
 1217 triggered by repeated events of smaller magnitude is similar to that done by larger, rarer events in this  
 1218 dataset, as revealed by the similar % of equivalent work done for years across a wide range of inferred  
 1219 recurrence interval.

1220

1221

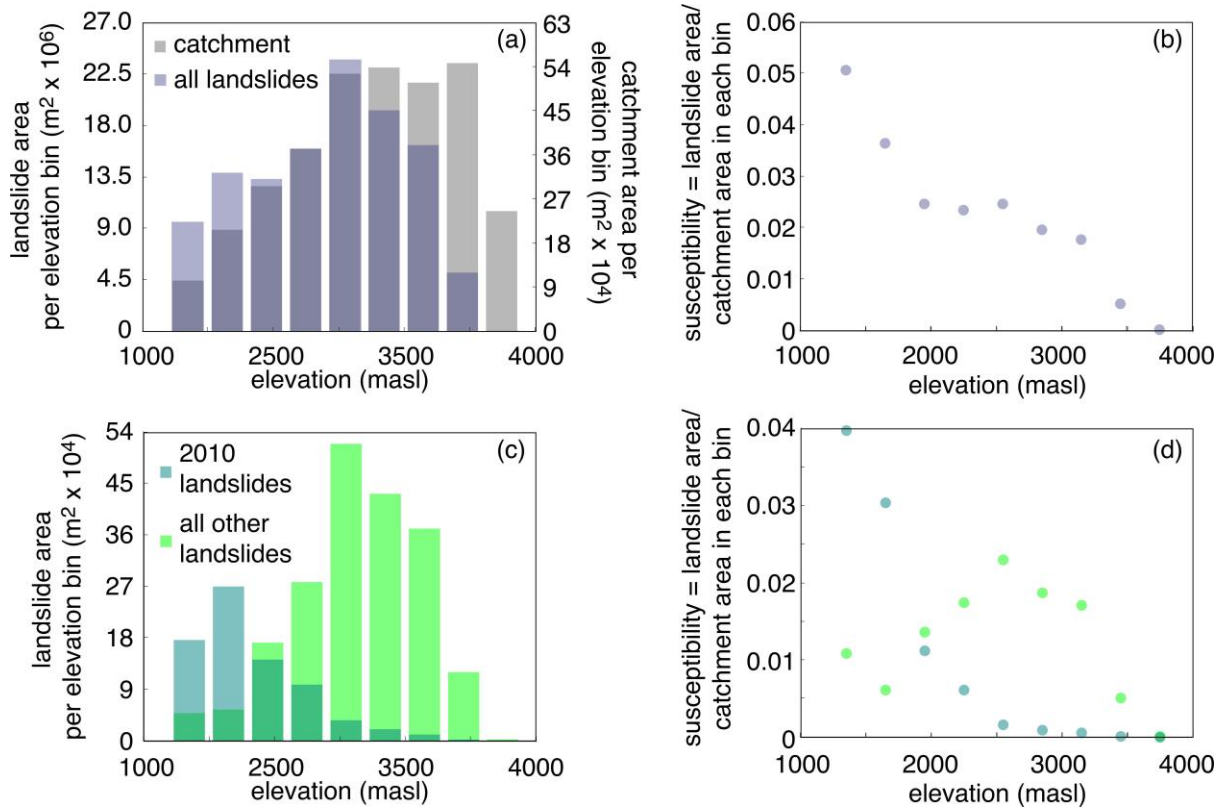


1222

1223 Figure 4: Landslide area-frequency diagram for all landslides mapped from 1988 to 2005 in a region  
 1224 of the Landsat image that overlapped with a Quickbird image from 2005, and for all landslides present  
 1225 in the Landsat visible region of the Quickbird image. The higher frequency of small landslides in the  
 1226 Quickbird inventory can be explained by the higher resolution of this image (2.4 m x 2.4 m, compared  
 1227 to 30 m x 30 m for Landsat). The power law tails of the two inventories are similar.

1228

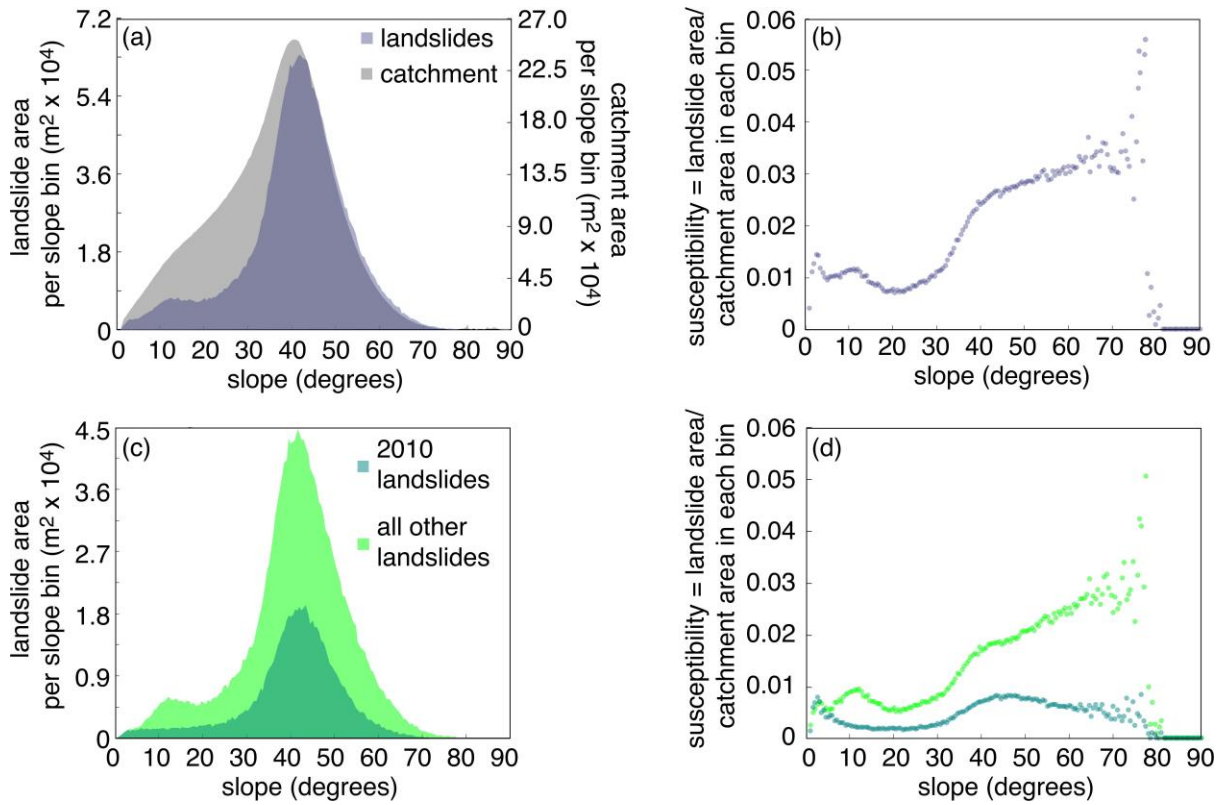




1229

1230 Figure 5: Histograms of catchment and landslide areas by elevation bins of 300 m: (a) all landslides in  
 1231 the 25-year dataset; (c) separating landslides occurring during 2010, associated with the large storm in  
 1232 March 2010, from those in the rest of the dataset. (b) and (d) Corresponding calculation of landslide  
 1233 susceptibility, calculated as the area of landslides within each bin divided by the total visible area in  
 1234 the Landsat images used for mapping.

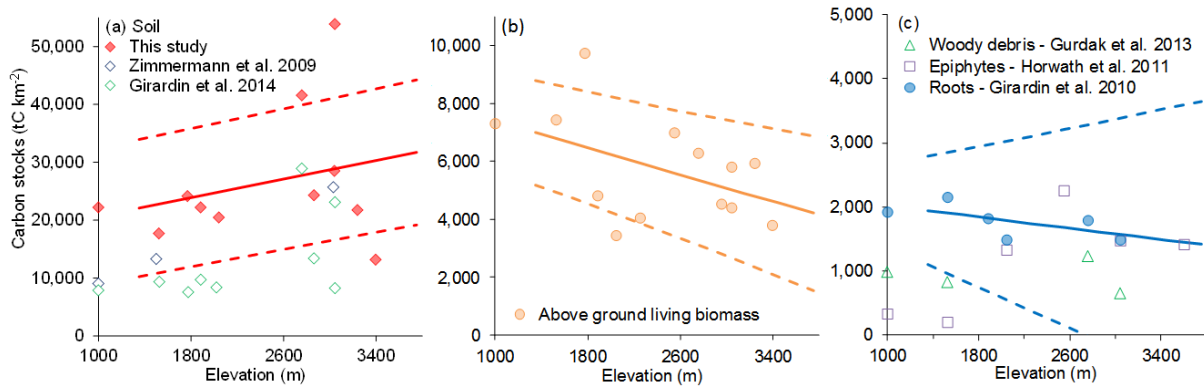
1235



1236

1237 Figure 6: Histograms of catchment and landslide areas by slope bins of  $1^\circ$ : (a) all landslides in the 25-  
 1238 year dataset; (c) separating landslides occurring during 2010, associated with the large storm in March  
 1239 2010, from those in the rest of the dataset. (b) and (d) Corresponding calculation of landslide  
 1240 susceptibility, calculated as the area of landslides within each bin divided by the total visible area in  
 1241 the Landsat images used for mapping.

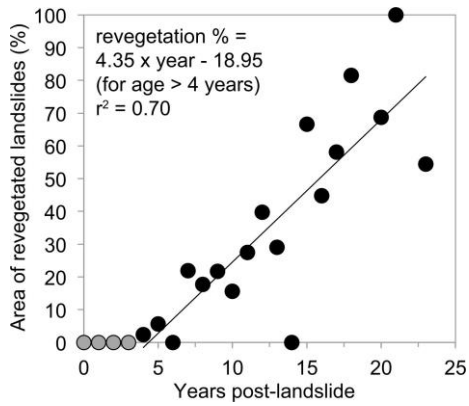
1242



1243

1244 Figure 7: Soil and vegetation carbon stocks ( $\text{tC km}^{-2}$ ) as a function of elevation for the tropical  
 1245 montane forest of Kosñipata Valley, in the eastern Andes of Peru (Girardin et al., 2014a; Gurdak et  
 1246 al., 2014; Horwath, 2011; Girardin et al., 2010; Zimmermann et al., 2009). Linear regressions  
 1247 generated from available carbon stock data ( $\text{tC km}^{-2}$ ) from the Kosñipata Valley for a) soil carbon  
 1248 stocks (red diamonds only; see Figure S1 and section 3.3.2. comparing the soil data with other  
 1249 datasets), b) above ground living biomass, and c) root biomass (Table 1). c) Woody debris, and  
 1250 epiphytes are shown for reference.

1251



1252

1253

Figure 8: Landslide revegetation time as percent area recovered by 2011, evaluated from a

1254

WorldView-2 pan-sharpened satellite image at 2 m x 2 m resolution. Each data point represents the

1255

landslides from a single year during the study period (black and grey circles; n = 23). Landslides

1256

occurring at least 4 years prior to 2011 (black circles) were used to calculate the best fit (area of

1257

revegetated landslides (%) =  $4.351 \pm 0.719 \times \text{year of landslide origin prior to 2011} - 18.953 \pm 9.974$ ,

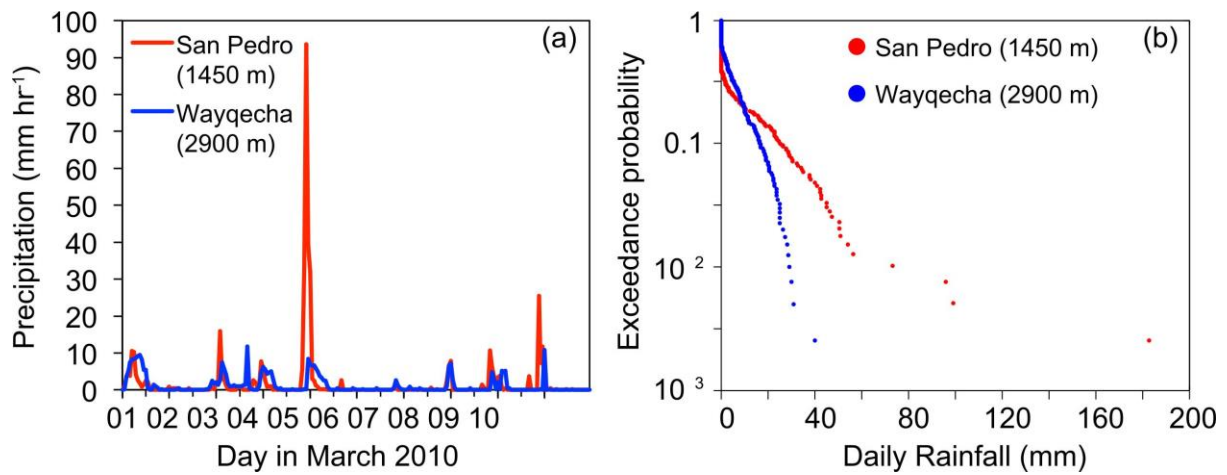
1258

where the mean estimated time for 100% revegetation of all the landslides of a given year is  $27 \pm 8$  yrs

1259

( $r^2 = 0.7$ , n = 18, p < 0.0001).

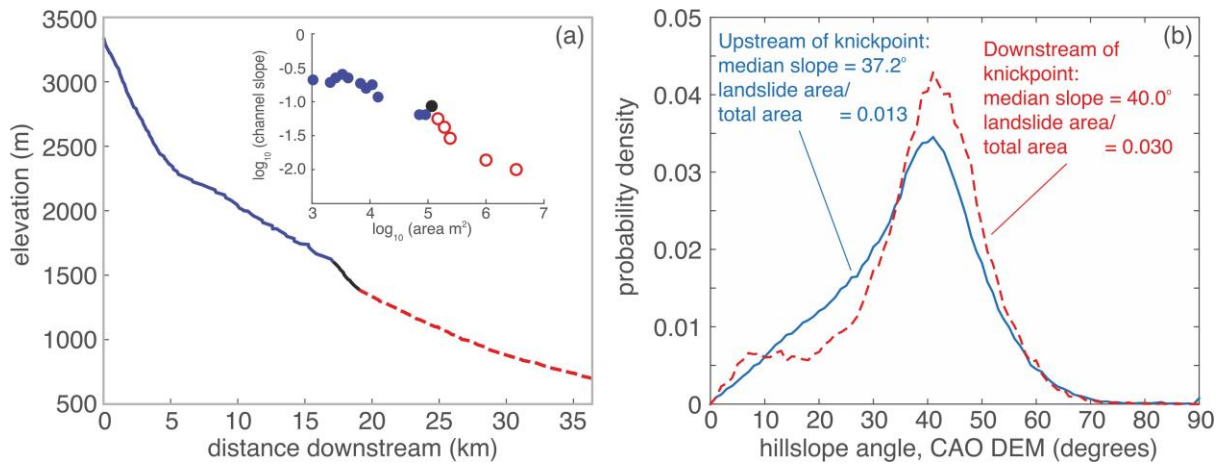
1260



1261

1262 Figure 9: (a) Precipitation during the March 2010 storm in the Kosñipata Valley at two stations, one at  
 1263 high elevation (Wayqecha plot, 2900 m), where storm precipitation was low, and another at low  
 1264 elevations (San Pedro, 1450 m; Clark et al., 2014; ACCA, 2012), where precipitation was high and  
 1265 where occurrence of storm-triggered landslides was also high (e.g., Fig. 5c). (b) Magnitude-frequency  
 1266 analysis of precipitation over multiple years at the two stations shown in (a), demonstrating that the  
 1267 low elevations in the Kosñipata study catchment are generally characterized by more low-frequency,  
 1268 high-magnitude precipitation events.

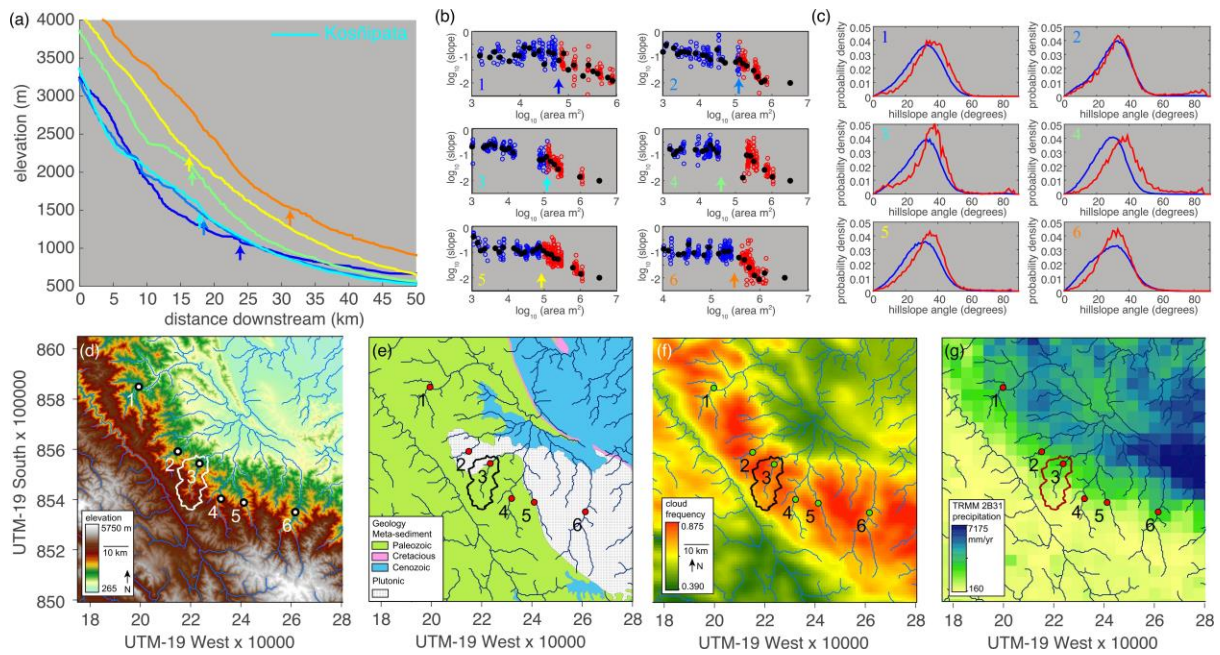
1269



1270

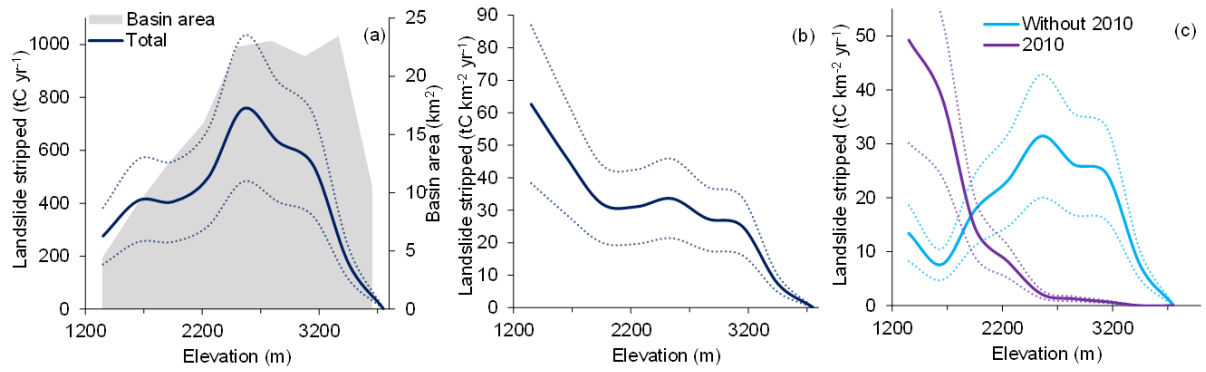
1271 Figure 10: (a) Longitudinal profile along the Kosñipata river channel, with a prominent vertical step  
 1272 knickpoint corresponding to (inset) a transition in the plot between channel slope and upstream  
 1273 contributing area, calculated following Moon et al. (2011). (b) Probability density of hillslope angles  
 1274 (from 3 m x 3 m CAO DEM) upstream and downstream of the morphological transition in the  
 1275 channel, along with median hillslope angles in each region and landslide susceptibility over the 25-  
 1276 year study period.

1277



1278

1279 Figure 11: (a-c) Analysis of river profiles analogous to those in Fig. 10 (shown here as River #3, in  
 1280 cyan), for rivers throughout the Alto Madre de Dios region (d). In (b), data are binned by upstream  
 1281 area and means are shown by black circles. Arrows in (a) refer to locations along the profile of  
 1282 observed transition in the area-slope plots (b). In (c), hillslope angles (from STRM DEM) are grouped  
 1283 by upstream (blue) and downstream (red) of this transition. Transition locations are displayed as dots  
 1284 in (d-g), which show regional elevation (Farr et al., 2007) (d), geology (INGEMMET, 2013) (e),  
 1285 Modis cloud frequency (Halladay et al., 2012) (f), and TRMM 2B31 annual precipitation (Bookhagen,  
 1286 2013) (g).

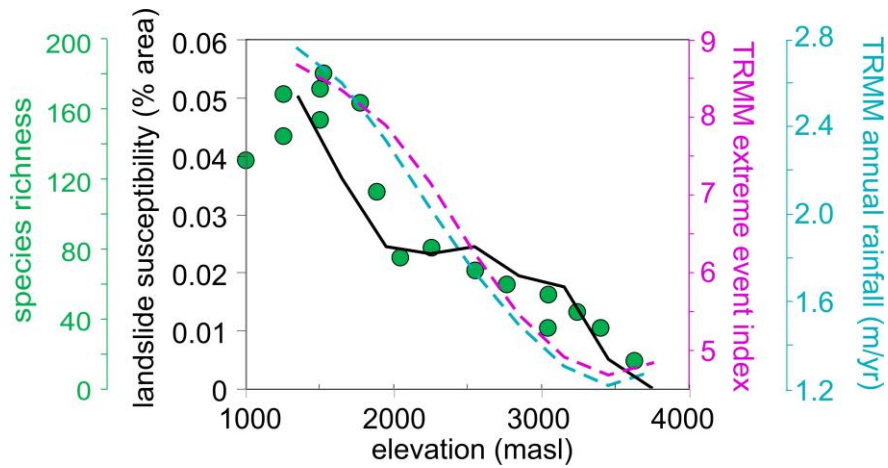


1287

1288 Figure 12: (a) Total mobilisation of organic carbon by landslides (tC yr<sup>-1</sup>) and (b) area-normalised  
 1289 mobilisation of organic carbon (tC km<sup>-2</sup> yr<sup>-1</sup>) over the altitudinal gradient divided into 300 m elevation  
 1290 bins contributed by the sum of soil and vegetation (total, navy line), with errors as dotted lines.  
 1291 Landslide susceptibility is highest at low elevations so the yield is highest there (b), but the total flux  
 1292 due to landslides is dominated by mid-elevations that comprise the majority of basin area (a). (c)  
 1293 Separation of landslide-mobilised organic carbon (tC km<sup>-2</sup> yr<sup>-1</sup>) due to the 2010 rain storm event from  
 1294 the remaining years as a function of elevation.

1295





1296

1297 Figure 13: Plots of landslide susceptibility, TRMM-based precipitation (both total annual precipitation  
 1298 and TRMM extreme event index) (Bookhagen, 2013), and species richness, as a function of elevation  
 1299 within the Kosñipata Valley. Note that absolute values of 2B31 TRMM annual precipitation are not  
 1300 accurate without calibration to meteorological station data (cf. Clark et al., 2014) but spatial patterns  
 1301 may be representative. Climatology, landslide occurrence, and species richness all generally increase  
 1302 from high to low elevations within the Kosñipata Valley, although landslide susceptibility and species  
 1303 richness show a discontinuous trend with elevation while TRMM-based climatology is more  
 1304 continuous.